Biogeosciences Discuss., 10, 3121–3175, 2013
www.biogeosciences-discuss.net/10/3121/2013/
doi:10.5194/bgd-10-3121-2013

Biogeosciences
Discussions
Open Access

Isotopic constraints on the pre-industrial oceanic nitrogen budget

C. J. Somes[1], A. Oschlies[1], and A. Schmittner[2]

[1]GEOMAR Helmholtz-Zentrum für Ozeanforschung Kiel, Düsternbrooker Weg 20,
24105 Kiel, Germany
[2]College of Earth, Ocean, and Atmospheric Sciences, Oregon State University,
104 CEOAS Admin Bldg., Corvallis, Oregon, 97331, USA

Received: 4 January 2013 – Accepted: 17 January 2013 – Published: 19 February 2013

Correspondence to: C. J. Somes (csomes@geomar.de)

Published by Copernicus Publications on behalf of the European Geosciences Union.

Abstract

The size of the bio-available (i.e. "fixed") nitrogen inventory in the ocean influences global marine productivity and the biological carbon pump. Despite its importance, the pre-industrial rates for the major source and sink terms of the oceanic fixed nitrogen budget, N_2 fixation and denitrification, respectively, are not well known. However, these processes leave distinguishable imprints on the ratio of stable nitrogen isotopes, $\delta^{15}N$, which can therefore help to infer their patterns and rates. Here we use $\delta^{15}N$ observations from the water column and a new database of seafloor measurements to constrain rates of N_2 fixation and denitrification predicted by a global three-dimensional Model of Ocean Biogeochemistry and Isotopes (MOBI). Sensitivity experiments were performed to quantify uncertainties associated with the isotope effect of denitrification in the water column and sediments. They show that the level of nitrate utilization in suboxic zones, that is the balance between nitrate consumption by denitrification and nitrate replenishment by mixing (dilution effect), significantly affects the isotope effect of water column denitrification and thus global mean $\delta^{15}NO_3^-$. Experiments with lower levels of nitrate utilization within the suboxic zone (i.e. higher residual water column nitrate concentrations, ranging from 20–32 µM) require higher ratios of benthic to water column denitrification (BD : WCD = 0.75–1.4, respectively), to satisfy the global mean NO_3^- and $\delta^{15}NO_3^-$ constraints in the modern ocean. This suggests that nitrate utilization in suboxic zones play an important role in global nitrogen isotope cycling. Increasing the net fractionation factor for benthic denitrification (ε_{BD} = 0–4 ‰) requires even higher ratios of benthic to water column denitrification (BD : WCD = 1.4–3.5, respectively). The model experiments that best reproduce observed seafloor $\delta^{15}N$ support the middle to high-end estimates for the net fractionation factor of benthic denitrification (ε_{BD} = 2–4 ‰). Assuming a balanced fixed nitrogen budget, we estimate that pre-industrial rates of N_2 fixation, water column denitrification, and benthic denitrification were approximately 195–345, 65–75, and 130–270 Tg N yr^{-1}, respectively. Although uncertainties still exist, these results suggest that previous estimates of N_2 fixation

BGD

10, 3121–3175, 2013

Isotopic constraints on the pre-industrial oceanic nitrogen budget

C. J. Somes et al.

have been significantly underestimated and the residence time for oceanic fixed nitrogen is between ~ 1500–3000 yr.

1 Introduction

Biotically available "fixed" nitrogen (fixed-N) is one of the major nutrients limiting phytoplankton growth in the ocean. Its generally low abundance in sunlit surface waters limits the primary production that forms the base of ocean ecosystems and provides energy for more complex, higher-level organisms (e.g. marine animals). Thereby, fixed-N also limits the biological sequestration of atmospheric carbon dioxide (CO_2) into biomass, part of which subsequently sinks towards the deep ocean. Respiration of organic matter back into CO_2 at depth affects the partitioning of CO_2 among the ocean and atmosphere, the so-called "biological carbon pump". It has been suggested that large changes in the oceanic fixed-N inventory can modulate the strength of the biological carbon pump and thereby influence atmospheric CO_2 over glacial/interglacial timescales (McElroy, 1983; Falkowski, 1997). Since processes that control the size of the fixed-N inventory are sensitive to climate (Gruber, 2004), they may have an important feedback on atmospheric CO_2 concentrations in past and future climates.

N_2 fixation, the conversion of N_2 gas into fixed-N by specialized microorganisms (diazotrophs), provides the ocean with most of its fixed-N. Other contributions to the fixed-N pool are from river input and atmospheric N deposition, which are estimated be approximately an order of magnitude lower than N_2 fixation in pre-industrial times (Galloway et al., 2004; Codispoti, 2007; Duce et al., 2008; Gruber, 2008). However, industrial N emissions and fertilizer production through the Haber-Bosch process that eventually cycles fixed-N into the atmosphere and rivers, have been steadily increasing in recent decades and are estimated to become comparable to "natural" N_2 fixation in following decades (Galloway et al., 2004).

Denitrification and anammox are the most important fixed-N removal processes in the ocean. They convert fixed-N into N_2 gas under suboxic conditions ($O_2 < \sim 10$ uM) in the water column and seafloor sediments. “Canonical” denitrification occurs when heterotrophic bacteria replace O_2 consumption with the reduction of nitrate (NO_3^-) to dinitrogen gas (N_2) as the electron acceptor during respiration, once O_2 is no longer available in sufficient quantity. Anammox, on the other hand, is a chemoautotrophic process that converts nitrite (NO_2^-) and ammonium (NH_4^+) into N_2 gas (Thamdrup and Dalsgaard, 2002; Kuypers et al., 2003). Since both denitrification and anammox processes occur in oxygen minimum zones (OMZs), the relative importance of each process is uncertain. Recent studies have found that water column denitrification dominates N-loss in the Arabian Sea (Ward et al., 2009; Bulow et al., 2010), while anammox is more important in the ETSP (Lam et al., 2009). However, Lam et al. (2009) estimates that the nitrate reduction, the first step of canonical denitrification, provides at least two-thirds of the nitrite that anammox consumes, suggesting that canonical denitrification may be the most important driver of total N-loss in OMZs. Therefore, we refer to denitrification as the major N-loss process in this paper.

While the major source and sink processes of the fixed-N budget, N_2 fixation and denitrification, respectively, are relatively well known, estimating their global rates remains a challenge. Estimates for N_2 fixation range widely between ~ 100–300 $\mathrm{Tg\,N\,yr^{-1}}$ as well as predicting different spatial patterns (Gruber and Sarmiento, 1997; Brandes and Devol, 2002; Karl et al., 2002; Deutsch et al., 2007; Monteiro et al., 2011; Eugster and Gruber, 2012). Methods historically used to measure N_2 fixation have been found to be underestimating N_2 fixation by as much as a factor of 2 (Mohr et al., 2010; Großkopf et al., 2012). Since new important N_2-fixing species are also still being discovered (Montoya et al., 2004; Foster et al., 2011; Zehr, 2011), more N_2 fixation could be taking place in the ocean than previously thought.

Global estimates of denitrification vary considerably as well. In the water column, studies suggest global rates between 50–150 $\mathrm{Tg\,N\,yr^{-1}}$ and in the sediments generally between 100–300 $\mathrm{Tg\,N\,yr^{-1}}$ (Middelburg et al., 1996; Galloway et al., 2004; Gruber, 2004; Codispoti, 2007; Bohlen et al., 2012; DeVries et al., 2012; Eugster and Gruber, 2012). Since the high-end estimates for denitrification are substantially larger than the high-end estimates for N_2 fixation, it has led to the debate whether the ocean could be rapidly losing as much as 400 Tg N yr^{-1} (Codispoti et al., 2001; Brandes and Devol, 2002; Codispoti, 2007), about 0.07 % of the total nitrate inventory per year, or whether the nitrogen budget is more balanced (Gruber and Sarmiento, 1997; Gruber, 2004; Altabet, 2007; Bianchi et al., 2012).

Stable nitrogen isotopes can provide constraints on N_2 fixation and denitrification because they leave distinguishable imprints on the ratio of oceanic $\delta^{15}N$, defined as $\delta^{15}N = [(^{15}N/^{14}N)_{sample}/(^{15}N/^{14}N)_{atmospheric} - 1] \cdot 1000‰$. Diazotrophs fix ^{15}N-depleted atmospheric N_2 into their biomass ($\delta^{15}N_{DIAZ} = -2–0‰$) relative to the deep ocean mean ($\delta^{15}NO_3^- = \sim 5‰$) (Sigman et al., 2000; Somes et al., 2010b). Denitrifying bacteria preferentially consume ^{15}N-depleted nitrate, the lighter and more reactive isotope, during water column denitrification ($\varepsilon_{WCD} = 20–30‰$), leaving the oceanic nitrate pool ^{15}N-enriched (Cline and Kaplan, 1975; Brandes et al., 1998; Voss et al., 2001). Benthic denitrification is observed to have a much lower net fractionation factor ($\varepsilon_{BD} = 0–3‰$), which is attributed to near complete NO_3^- utilization in pore-water sediments (Brandes and Devol, 2002; Lehmann et al., 2004). However, recent studies (Lehmann et al., 2007; Granger et al., 2011; Alkhatib et al., 2012) investigating fractionation involved with the nitrification-denitrification loop in the sediments suggest a larger net fractionation factor for benthic denitrification ($\varepsilon_{BD} = 4–8‰$). The global ocean mean $\delta^{15}NO_3^-$ provides a constraint on the fixed-N budget because the combination of the different isotope effects of N_2 fixation and total denitrification, along with their respective rates, determines global mean $\delta^{15}NO_3^-$ (Brandes and Devol, 2002).

Global nitrogen isotope models can estimate the relative rates of N_2 fixation, water column and benthic denitrification required to match the global ocean mean $\delta^{15}NO_3^-$. The input of ^{15}N-depleted nitrogen from N_2 fixation must compensate for the preferential removal of ^{15}N-depleted nitrate by denitrification. Assuming constant isotope effects for water column and benthic denitrification, one can calculate the relative rates needed to match this observational constraint. For example, when using a fractionation factor of

0 ‰ for benthic denitrification, it will not directly affect the nitrogen isotopes. However, benthic denitrification will stimulate additional N_2 fixation assuming a balanced fixed-N budget. Then it can be calculated how much "extra" N_2 fixation needs to be stimulated by benthic denitrification to balance the ^{15}N-enriched nitrate produced by water column denitrification.

Modeling studies that take into account these different isotope effects to constrain rates of N_2 fixation and denitrification have produced differing results. For example, Brandes and Devol (2002) used a one-box model to calculate the rates of N_2 fixation and denitrification needed to obtain the observed global mean $\delta^{15}\mathrm{NO}_3^-$, using fractionation factors of 1.5 ‰, and 25 ‰ for benthic denitrification and water column denitrification, respectively. They estimated that a ratio of benthic to water column denitrification (BD : WCD) of ~ 3.7 : 1 is required to achieve the observed oceanic mean $\delta^{15}\mathrm{NO}_3^-$, supporting the high-end estimates for benthic denitrification.

Other studies have used more complex box models to investigate global nitrogen isotope cycling (Deutsch et al., 2004; Eugster and Gruber, 2012). They found that it is important to account for the locally reduced nitrate concentrations in suboxic zones that mix into surrounding oxic waters with higher nitrate. Since the mixed $\delta^{15}\mathrm{NO}_3^-$ value will be weighted towards the higher nitrate concentration, the local utilization of nitrate reduces the influence of the ^{15}N-enriched nitrate from water column N-loss on the global mean $\delta^{15}\mathrm{NO}_3^-$, a mechanism referred to as the "dilution effect" (Deutsch et al., 2004). This conservation of mass is implicit within the physical transport terms (i.e. mixing, advection) of ocean circulation models. These studies assume fractionation factors of 0 ‰, and 25 ‰ for benthic denitrification and water column denitrification, respectively, in their model and estimate that a lower BD : WCD ratio of 1.8–2.7 compared to the Brandes and Devol (2002) of ~ 3.7 : 1 would be required to satisfy the global ocean $\delta^{15}\mathrm{NO}_3^-$ when the dilution effect is taken into account.

Altabet (2007) used a one-box model approach, but parameterized the isotope effects of local nitrate utilization and dilution during water column denitrification. He argues that these effects would further reduce the isotope effect of water column denitrification by ~13 ‰ compared to the inherent microbial process near 25 ‰. Applying this reduced isotope effect for water column denitrification (~12 ‰), and 0 ‰ for benthic denitrification, respectively, he estimated that the BD : WCD ratio should be ~1 : 1. These box model studies highlight how sensitive the global ocean mean $\delta^{15}NO_3^-$ can be to different assumptions made for the isotope effects of N-denitrification, and their associated rates needed to achieve the observed global mean $\delta^{15}NO_3^-$.

In this study, we go beyond earlier box-model approaches and employ a global coupled circulation-biogeochemistry-isotope model to investigate to what extent rates of N_2 fixation and denitrification can be constrained by $\delta^{15}N$ observations in the water column and seafloor sediments. In particular, we will investigate the uncertainties associated with (i) the effects of nitrate utilization and dilution on the isotope effect of water column denitrification and (ii) the net fractionation factor associated with benthic denitrification. In addition to water column $\delta^{15}NO_3^-$ observations, a new global seafloor sediment $\delta^{15}N$ database (Tesdal et al., 2013) is used to evaluate the model experiments. The rates of N_2 fixation and denitrification implicit in the model simulations that perform superior with respect to observed $\delta^{15}NO_3^-$ and seafloor $\delta^{15}N$ then provide our best estimate of N_2 fixation and denitrification in the real ocean.

2 Model description

The global coupled Model of Ocean Biogeochemistry and Isotopes (MOBI) used is based on the version of Somes et al. (2010b). A technical description of the model is located in Appendix B and a brief overview is provided below.

2.1 Physical model

The physical model is based on the University of Victoria Earth System Climate Model (Weaver et al., 2001), version 2.9 (Eby et al., 2009). It includes a global, three-dimensional general circulation model of the ocean (Modular Ocean Model 2) with physical parameterizations such as diffusive mixing along and across isopycnals, eddy induced tracer advection (Gent and McWilliams, 1990), the computation of tidally induced diapycnal mixing over rough topography (Simmons et al., 2004), and an anisotropic viscosity scheme (Large et al., 2001) in the tropics. Nineteen vertical levels are used with a horizontal resolution of $1.8^\circ \times 3.6^\circ$. A two dimensional, single level energy-moisture balance model of the atmosphere and a dynamic-thermodynamic sea ice model are used, forced with prescribed NCEP/NCAR monthly climatological winds (Kalnay et al., 1996).

2.2 Biogeochemical-ecosystem model

MOBI is an improved version of the model used in Somes et al. (2010b) (see Fig. 1). The organic compartments include two classes of phytoplankton, N_2-fixing diazotrophs (P_D) and an "ordinary" nitrate assimilating phytoplankton class (P_O), as well as zooplankton (Z), and sinking detritus (D). The inorganic variables include dissolved oxygen (O_2) and two nutrients, nitrate (NO_3^-) and phosphate (PO_4^{3-}), both of which are consumed by phytoplankton.

This model version deviates from that of Somes et al. (2010b) by including varying elemental stoichiometry. While general phytoplankton N : P remains at the canonical Redfield ratio (N : P = 16), diazotroph N : P is set to 40, which is in better agreement with most observations (N : P = 20–50+) (Letelier and Karl, 1998; Sanudo-Wilhelmy et al., 2004), as well as an optimality-based growth model (Klausmeier et al., 2004). This allows diazotrophs to more efficiently fix N_2 into the ocean when they are P-limited, but does not significantly change the pattern of N_2 fixation. Since zooplankton are capable of maintaining their own stoichiometry (Sterner and Elser, 2002), we set zooplankton N : P to 16 : 1 and assume that they excrete excess N when grazing diazotrophs. Detrital N and P are explicitly calculated as separate prognostic variables. The C : N ratio for all compartments is held constant at C : N = 6.625.

2.2.1 N_2 fixation

Diazotrophs grow according to the same principles as the general phytoplankton class in MOBI, but we account for their different characteristics. N_2 fixation is energetically more costly than assimilating fixed-N. Diazotrophs must break down the strong triple-N bond and undergo extra respiration to keep the N_2-fixing compartment anoxic since O_2 inhibits the expression of the N_2-fixing gene (nifH). Thus, the growth rate of diazotrophs is reduced compared to ordinary phytoplankton by a handicap factor ($c_{\mathrm{Diaz}} = 0.13$). Diazotroph growth is not explicitly set to 0 at 15 °C as in previous model versions (Schmittner et al., 2008a; Somes et al., 2010b), but are now allowed to grow at low rates in cooler waters according to Eq. (B4), consistent with culture experiments (Pandey et al., 2004; Le Quéré et al., 2005).

Diazotrophs are not limited by nitrate and can out-compete general phytoplankton in surface waters that are depleted in fixed-N, but still contain sufficient P and Fe (i.e. water with low nitrate from N-loss and high atmospheric Fe deposition). They will consume nitrate if available, consistent with culture experiments (Mulholland et al., 2001; Holl and Montoya, 2005), which is another factor that inhibits N_2 fixation in high-nutrient low-chlorophyll (HNLC) regions in the model. Diazotroph prey-capture rate is also reduced relative to the general phytoplankton class to account for lower grazing on diazotrophs versus other phytoplankton (Table A1) (Mulholland, 2007), which was at an equal level in Somes et al. (2010b).

Due to uncertainties in modeling the iron cycle (Aumont et al., 2003; Moore et al., 2004; Galbraith et al., 2010), iron is currently not included as a prognostic tracer. Instead, a monthly Fe limitation mask is calculated based on aeolian Fe deposition estimates (Mahowald et al., 2005a, 2006, 2009). This Fe mask is multiplied to diazotroph's maximum growth rate to account for Fe limitation (Somes et al., 2010a).

2.2.2 Water column denitrification

Water column denitrification occurs when organic matter is respired under suboxic conditions. It is parameterized in MOBI according to Eq. (B11) that determines the relative amount of nitrate consumption that takes place during respiration at low ambient oxygen concentrations. We use a threshold of 5 µM O_2 that sets the level where respiration by denitrification overtakes aerobic respiration (Fig. B1). This parameterization was designed to best capture the decreasing $NO_3^- : PO_4^{3-}$ ratios in suboxic zones. Anammox is also removing fixed-N in these areas of low oxygen and high organic matter recycling. Although the exact partitioning between water column denitrification and anammox is not well known, anammox likely depends on the first step of denitrification ($NO_3^- \rightarrow NO_2^-$) to supply sufficient nitrite that typically exists in very low concentrations (Lam et al., 2009). Since MOBI does not differentiate between different species of dissolved inorganic nitrogen, this water column denitrification parameterization is designed to implicitly capture total fixed-N loss from both canonical water column denitrification and anammox.

2.2.3 Benthic denitrification

Benthic denitrification is included using a new empirical function deduced from benthic flux measurements (Bohlen et al., 2012). This function estimates denitrification in the sediments based on organic carbon rain rate into the sediments, and bottom water O_2 and NO_3^- concentrations (Eq. B12). It provides an efficient alternative to coupling a full sediment model that would significantly reduce simulation speed. Note that all organic matter instantaneously remineralizes in the bottom water when it hits the seafloor sediment interface. Nitrate is then removed from the bottom water according to this benthic denitrification function. While the organic carbon rain rate predicts benthic denitrification rates to first-order, Bohlen et al. (2012) found a strong non-linear relationship to the empirical parameter $O_2^* = O_2 - NO_3^-$ parameter of oxygen and nitrate concentrations in the bottom water overlying the sediments. Benthic denitrification rates are significantly higher as O_2^* decreases (i.e. when O_2 is low and NO_3^- is high) for similar organic carbon rain rates. We also include sub-grid scale bathymetry within this benthic denitrification scheme to account for shallow continental shelves and other topographical features that are not fully resolved in MOBI's coarse-resolution grid (see Appendix B).

2.3 Nitrogen isotope model

The nitrogen isotope model simulates the two stable nitrogen isotopes, ^{14}N and ^{15}N, in all N species included in the marine ecosystem model. Fractionation results in the preferential incorporation of the more reactive, thermodynamically preferred ^{14}N isotope into the product of each reaction by a process-specific fractionation factor, α (Mariotti et al., 1981). We report these values in the more commonly used "δ" notation, where the fractionation factor takes the form $\varepsilon = (1-\alpha) \times 1000$. The processes in the model that fractionate nitrogen isotopes are phytoplankton nitrate assimilation ($\varepsilon_{\text{assim}} = 5\,‰$), N_2 fixation ($\varepsilon_{\text{Nfix}} = 1.5\,‰$), zooplankton excretion ($\varepsilon_{\text{excr}} = 6\,‰$), water column denitrification ($\varepsilon_{\text{WCD}} = 25\,‰$), and benthic denitrification ($\varepsilon_{\text{BD}} = 0, 2, 4\,‰$). For example, diazotroph biomass becomes 1.5 ‰ depleted in $\delta^{15}N$ relative to the source (atmospheric $\delta^{15}N_2 = 0\,‰$) giving diazotroph biomass a $\delta^{15}N$ signature of $-1.5\,‰$ when they fix atmospheric N_2 for growth.

We refer to the fractionation factor as the ε value chosen for the fractionation equation and the "isotope effect" as the overall effect the process has on the $\delta^{15}N$ distribution in the ocean. The total isotope effect also includes effects from source values and processes that alter the impact of the net fractionation, such as nitrate utilization and dilution. N_2 fixation, for example, has a low fractionation factor, but a strong isotope effect by introducing very ^{15}N-depleted nitrogen ($\delta^{15}N_{\text{Nfix}} = -1.5\,‰$) into the oceanic fixed-N pool relative to deep ocean mean $\delta^{15}NO_3^-$ near 5 ‰. In MOBI, fractionation factors are constant in space and time, and chosen to best represent estimates from field observations (Somes et al., 2010b).

2.4 Nitrogen isotope sensitivity experiments

The model experiments were initialized with World Ocean Atlas 2009 (WOA09) observations (temperature, salinity, oxygen, nitrate, and phosphate) (Antonov et al., 2010; Garcia et al., 2010a,b; Locarnini et al., 2010) and integrated for over 10 000 yr with pre-industrial boundary conditions as the nitrogen cycle approached equilibrium. While the scarcity of water column observations makes it difficult to estimate global mean $\delta^{15}NO_3^-$, vertical $\delta^{15}NO_3^-$ profiles throughout the global ocean converge to ∼5 ‰ at depths below 2000 m (Somes et al., 2010b), which is the $\delta^{15}NO_3^-$ setting used to constrain the model. Here the following uncertain parameters were adjusted such that the global mean deep ocean (2–6 km) $\delta^{15}NO_3^- \sim 5$ ‰ and global $NO_3^- \sim 30.8$ µM: factor α_{BD}, which determines total benthic denitrification rate; prey-capture, ϖ_{Diaz}, and mortality, ν_{Diaz}, rates of diazotrophs, both impacting N_2 fixation (Tables 1, 2). In the following annual mean results from the final 500 yr of the integrations are reported.

2.4.1 Water column denitrification experiments

This set of experiments was designed to test the importance of the isotope effect of water column denitrification on the global ocean mean $\delta^{15}NO_3^-$. We follow a method introduced by Moore and Doney (2007) that limits the rate of water column denitrification (lim WCD) at given nitrate thresholds of 20, 26, and 32 µM (Table 2, Fig. 2). These values were chosen to produce water column denitrification rates that lie within the range of modern estimates between 70–150 Tg N yr^{-1}. Note only the highest threshold applied (lim WCD = 32) captures the average nitrate concentration in the suboxic zones suggested by WOA09 (∼32 µM), while the other experiments underestimate nitrate there. Models with higher thresholds also have lower levels of nitrate utilization in the suboxic zones that influences the isotope effect of water column denitrification. In order to exclude impacts on the distribution of other biogeochemical tracers (oxygen, phosphate), remineralization of organic matter was left unchanged in these sensitivity experiments. Only nitrate consumption during water column denitrification was turned off below the respective nitrate threshold.

2.4.2 Benthic denitrification fractionation experiments

Field studies estimate the fractionation factor of benthic denitrification to be much smaller than that of water column denitrification, but to what extent still remains uncertain. The small increase in bottom water $\delta^{15}NO_3^-$ overlying benthic denitrification zones suggests the fractionation factor should be in the range 0–3 ‰ (Brandes and Devol, 2002; Lehmann et al., 2004). However, more recent studies have suggested a much higher net fractionation for benthic denitrification (Lehmann et al., 2007; Granger et al., 2011; Alkhatib et al., 2012). They suggest the ^{15}N-enriched ammonium measured in the overlying bottom water, presumably released from the sediments, was due to fractionation during the nitrification-denitrification loop in the sediments. These studies indicate a net fractionation factor for benthic denitrification in the range 4–8 ‰. We performed experiments with benthic denitrification net fractionation at 0, 2, and 4 ‰ to test its effect on the global nitrogen isotope budget.

3 Results

3.1 Patterns of N_2 fixation and denitrification

3.1.1 N_2 fixation

Diazotrophs perform N_2 fixation primarily in the tropics/subtropics where sufficient atmospheric Fe deposition occurs (e.g. North Atlantic, Western Pacific, and North Indian Ocean). Besides temperature and Fe availability, another important factor that determines where model diazotrophs are most abundant include competition for resources with other phytoplankton (i.e. N- vs. P-limitation). Denitrification consumes nitrate and increases N-limitation “downstream” of denitrification zones. In MOBI, this creates ecological niches for diazotrophs because they are not limited by nitrate. Nitrate depletion at the surface thus stimulates N_2 fixation as long as temperatures are high enough and sufficient Fe and P is available (Fig. 2). The spatial pattern of N_2 fixation is similar in all experiments, but with differing rates depending on the denitrification rate in each experiment.

3.1.2 Water column denitrification

Water column denitrification occurs when organic matter is respired in suboxic zones. This occurs in the Eastern Tropical North/South Pacific, the Bay of Bengal, and the Eastern Tropical Atlantic in MOBI (Fig. 2). Note that in the real ocean, large rates of water column denitrification also occur in the Arabian Sea, which is not reproduced in the model. Instead, the model displaces the suboxic zone to the Bay of Bengal, which is very close to the suboxic threshold in nature. Similar discrepancies between simulated and observed regions of water column denitrification in the Indian Ocean have also been found in other models (Moore and Doney, 2007; Gnanadesikan et al., 2012). Its causes are not fully understood and may include a misrepresentation of coastal currents or precipitation in the Indian Ocean. Although denitrification is not regularly observed in the Atlantic Ocean, anammox bacteria have been found in the Eastern Tropical South Atlantic suggesting that N-loss events can occur there (Kuypers et al., 2005). Nevertheless, the model seems to significantly overestimate water column N-loss in the Atlantic Ocean.

3.1.3 Benthic denitrification

Benthic denitrification occurs where large amounts of particulate organic carbon (POC) sink into the seafloor sediments, primarily along on the continental shelves and slopes (Middelburg et al., 1996; Bohlen et al., 2012). Since these exist in all ocean basins, benthic denitrification has a more global distribution compared to water column denitrification that is predominant in three distinct tropical suboxic regions (Fig. 2). The percentage of total benthic denitrification (including α_{BD}) simulated on the continental shelves (0–150 m), slopes (150–2000 m), and deep seafloor (2000–6000 m) is 35 %, 45 %, and 20 %, respectively, which does not vary by more than ±5 % for the different model experiments.

3.2 Observational δ^{15}N constraints

3.2.1 Seafloor δ^{15}N

We compare sinking δ^{15}N in the model with a new global database of seafloor δ^{15}N (Tesdal et al., 2013) (Fig. 3). It is composed of 2347 bulk δ^{15}N measurements covering all ocean basins. This seafloor δ^{15}N database provides a more complete view of the global nitrogen isotope distribution compared to available water column $\delta^{15}NO_3^-$ observations, which are sparse in space and time (Somes et al., 2010b). Since seafloor δ^{15}N measurements represent the accumulation of material spanning the last hundreds to thousands of years, they remove seasonal, interannual, or anthropogenic variability that can impact any single water column observation, making seafloor δ^{15}N an ideal dataset to constrain the long-term average of the pre-industrial ocean.

Diagenetic alteration of δ^{15}N occurs as sinking δ^{15}N becomes buried in seafloor sediments, which can potentially bias the interpretation of bulk sediment δ^{15}N. However, an analysis investigating diagenetic δ^{15}N alteration shows a clear relationship with water depth (Robinson et al., 2012). Data at > 50 sites where sinking δ^{15}N from traps were compared to seafloor δ^{15}N show a ~ 0.8–1 ‰ δ^{15}N diagenetic increase per kilometer of water depth. We accordingly adjust the model sinking δ^{15}N of the particulate organic nitrogen (PON) hitting the seafloor by increasing its values by 0.9 ‰ km^{-1} to account for diagenetic δ^{15}N alteration that is not incorporated into MOBI. This diagenetic enrichment increases the globally averaged δ^{15}N-PON into the sediments by 3.36 ‰ in the model experiments performed here and makes global mean values consistent with the observations (Table 3). The data-masked global seafloor δ^{15}N average varies somewhat depending on rates of N_2 fixation and denitrification in the different model experiments, but all model experiments show similar values across the Southern Ocean (Table 3), which is not significantly affected by denitrification and N_2 fixation.

MOBI reproduces the major trends of the seafloor δ^{15}N dataset (Fig. 3). The isotope effects of phytoplankton NO_3^- assimilation, water column denitrification, and N_2 fixation drive these large-scale patterns of δ^{15}N in the model. Relatively ^{15}N-depleted sinking nitrogen hitting the seafloor ($\delta^{15}N = 0$–4 ‰) occur in High Nutrient Low Chlorophyll (HNLC) regions of the Southern Ocean and Eastern Equatorial Pacific where NO_3^- utilization by phytoplankton is low. Here phytoplankton are able to preferentially incorporate ^{15}N-depleted nitrate into its biomass due to high availability of nitrate ($\varepsilon_{\text{assim}} = 5$ ‰). The nitrate utilization isotope effect also produces more ^{15}N-enriched nitrate in surface waters as utilization increases. In the subtropical gyres where nitrate is nearly fully utilized, phytoplankton must consume this ^{15}N-enriched nitrate remaining in the surface water, causing much higher sinking δ^{15}N values there (> 6 ‰), in the absence of N_2 fixation. All model experiments produce similar patterns and regional averages across the Southern Ocean where surface NO_3^- utilization dominates the δ^{15}N trend (Table 3, Fig. 4).

Very high seafloor δ^{15}N values (> 10 ‰) are observed near suboxic zones due to the large fractionation factor of water column denitrification. Modeling the correct extent of the suboxic zones remains a challenge in global coarse-resolution models due to the limited spatial extent of suboxic zones. While the suboxic zones are generally simulated in the correct ocean basins (e.g. Eastern Tropical Pacific, Northern Indian), they are all too large and displaced in the model. Since water column denitrification has a strong local effect on δ^{15}N, this displacement causes rather poor model fits when comparing to the seafloor δ^{15}N database (e.g. $r < 0.6$, Table 3). If all OMZ regions with less than 30 µM dissolved O_2 are not included when calculating the global metrics, the correlation coefficient increases from 0.59 to 0.68 (in model experiment #4), showing that the bias due to the displaced suboxic zones is one of the main deficiencies of the model. The model experiments that contain the lowest amount of water column denitrification (lim WCD = 32) represent the seafloor δ^{15}N database the best (Table 3, Fig. 4).

N_2 fixation introduces ^{15}N-depleted nitrogen (δ^{15}N = −1.5 ‰) into the ocean. It occurs primarily in tropical/subtropical waters "downstream" of denitrification zones where nitrate has been depleted and aeolian Fe deposition is high. Aeolian Fe deposition is generally higher in the western portion of the ocean basins and also with greater magnitude in the northern hemisphere. In MOBI, this causes a trend of lower sinking δ^{15}N values in the northern subtropical gyres, which is supported by the observational seafloor δ^{15}N (Fig. 3), as well as water column observations (Somes et al., 2010a).

Lowest values of seafloor δ^{15}N occur in the North Atlantic, which is known to support high rates of N_2 fixation (Karl et al., 2002). The model experiment that best reproduces these low values there has the highest rate of global N_2 fixation (Fig. 4). This model experiment also has the highest rate of benthic denitrification, which removes fixed-N at high latitudes and stimulates additional N_2 fixation in subtropical gyres (Fig. 2). Note that atmospheric nitrogen deposition is not included in this model version. Since pre-industrial deposition rates are estimated to be approximately an order magnitude lower than N_2 fixation (Duce et al., 2008), it likely has a small effect in this pre-industrial scenario. However, atmospheric N deposition can introduce even more ^{15}N-depleted nitrogen in the North Atlantic (δ^{15}N ~ −4 ‰) (Ryabenko et al., 2012), which could bias the model-data comparison.

The Subarctic Oceans contain large, shallow shelves where benthic denitrification occurs. Seafloor δ^{15}N show higher values (6–10 ‰) towards the shallow shelves in the Bering Sea, Sea of Okhotsk, Baffin Bay, and Banks of Newfoundland, despite the fact that less enrichment during burial occurs on these shallow shelves (Robinson et al., 2012). The model experiment with the largest net fractionation factor for benthic denitrification (ε_{BD} = 4 ‰) best reproduces the observational trends of high seafloor δ^{15}N in these areas (Fig. 4) although values are still slightly underestimated. The other model experiments with smaller fractionation factors produced too low δ^{15}N throughout this region. Some of the bias in this region may also be due to the shallow continental shelves that are not fully resolved in MOBI, nor the small-scale processes that take place on them. This could significantly affect surface NO_3^- utilization pattern, and thus seafloor δ^{15}N. Future model versions with higher vertical resolution will evaluate this potential model bias. Nevertheless, this model-data comparison supports the view of net fractionation factors for benthic denitrification to be ≥ 4 ‰, at least in the shallow Subarctic Ocean.

3.2.2 Water column $\delta^{15}NO_3^-$

The global ocean mean $\delta^{15}NO_3^-$ is determined by the rates and isotope effects of the source and sink terms of the fixed-N budget: N_2 fixation, water column denitrification, and benthic denitrification. N_2 fixation provides the ocean with ^{15}N-depleted nitrogen ($\delta^{15}N_{Nfix} = -1.5$ ‰). N-loss processes, on the other hand, preferentially consumes this ^{15}N-depleted nitrogen, leaving the global mean nitrate pool enriched in ^{15}N (global mean $\delta^{15}NO_3^- = \sim 5.5$ ‰) (Table 2). The average net fractionation that occurs during total N-loss determines how high the global mean $\delta^{15}NO_3^-$ will be relative to the ^{15}N-depleted nitrogen source from N_2 fixation. We focus on two isotope effects with high uncertainty in this study: (i) OMZ nitrate utilization and dilution impacts on the isotope effect of water column denitrification and (ii) the net fractionation factor associated with benthic denitrification.

(i) OMZ nitrate utilization and dilution isotope effect

The elevated $\delta^{15}NO_3^-$ signature produced in suboxic zones depends on the level of nitrate utilization there. Utilization is determined by the balance between consumption by denitrification and replenishment by mixing. This balance determines the average $\delta^{15}NO_3^-$ value that denitrifiers consume and convert to N_2 gas. The dilution effect takes into account that $\delta^{15}NO_3^-$ will be weighted towards the water parcel with higher nitrate when mixing occurs. For example, if the nitrate concentration in the suboxic zone is only half of the nitrate concentration in surrounding oxic waters, the $\delta^{15}NO_3^-$ signature of the oxic water will have twice the influence on total $\delta^{15}NO_3^-$ of these water masses if they mix together. Note that the dilution effect is implicitly simulated in the physical circulation model.

High levels of nitrate utilization reduce the influence of the isotope effect of water column denitrification on global mean $\delta^{15}\mathrm{NO}_3^-$. As average $\delta^{15}\mathrm{NO}_3^-$ increases in suboxic zones as denitrification occurs, the nitrate removed then becomes more ^{15}N-enriched. The influence of the isotope effect of water column denitrification on global mean $\delta^{15}\mathrm{NO}_3^-$ is reduced when the removed nitrogen has a higher δ^{15}N signature that is closer to global mean $\delta^{15}\mathrm{NO}_3^-$.

For example, imagine a situation with high nitrate utilization in which the average $\delta^{15}\mathrm{NO}_3^-$ value in the suboxic zone was 30.5 ‰ (instead of ~ 12–15 ‰ in the real ocean). The nitrogen removed would then have an isotopic signature 25 ‰ depleted relative to this value, which would be equal to the global mean ($\delta^{15}\mathrm{N}_{\mathrm{removed}} = 5.5$ ‰). In this case, it would have no influence on global mean $\delta^{15}\mathrm{NO}_3^-$, even though denitrification is still fractionating the nitrogen isotopes. Thus, as nitrate utilization increases the $\delta^{15}\mathrm{NO}_3^-$ signature of the suboxic zone, it reduces the influence of water column denitrification on global mean $\delta^{15}\mathrm{NO}_3^-$.

Experiments with high nitrate utilization in the suboxic zone require less N_2 fixation, and thus lower ratios of benthic to water column denitrification (BD : WCD), to maintain global mean $\delta^{15}\mathrm{NO}_3^-$ with a balance fixed-N budget. The nitrate utilization effect alone (varying lim WCD) required BD : WCD ratios that varied by nearly a factor of 2 in our range of sensitivity experiments (Table 2). Benthic denitrification is needed in the model to stimulate additional N_2 fixation to balance global mean $\delta^{15}\mathrm{NO}_3^-$ to the observed level. When nitrate utilization is high, the influence of the isotope effect of water column denitrification is reduced and therefore less benthic denitrification, and lower BD : WCD ratios, are required to balance global mean $\delta^{15}\mathrm{NO}_3^-$.

The model experiment that best reproduces nitrate and $\delta^{15}\mathrm{NO}_3^-$ observations in the suboxic zone is lim WCD = 32 (Table 2, Fig. 5). It gives a good agreement with the amount of nitrate drawdown, as well as the slope of the increasing $\delta^{15}\mathrm{NO}_3^-$ as nitrate is consumed according to off-shelf observations in suboxic zones. The experiments with higher levels of nitrate utilization (lim WCD = 20, 26) show too much nitrate consumption there. Due to deficiencies in the simulated suboxic zones, it still cannot be confirmed if the balance between nitrate consumption and replenishment is completely consistent with suboxic zones in the real ocean and the lim WCD = 32 experiment. However, the high sensitivity of estimated rates of N_2 fixation and denitrification in our model experiments that test different levels of nitrate utilization suggests nitrate utilization plays an important role in global nitrogen isotope cycling. This highlights the need for higher resolution models that fully resolve all of the ventilation pathways (e.g. coastal undercurrents and eddies) of suboxic zones.

(ii) Isotope effect of benthic N-loss

Recent studies (Lehmann et al., 2007; Granger et al., 2011; Alkhatib et al., 2012) have suggested a higher net fractionation factor associated with benthic denitrification ($\varepsilon_{BD} = 4$–8 ‰) compared to previous estimates ($\varepsilon_{BD} = 1$–3 ‰) (Brandes and Devol, 2002; Lehmann et al., 2004). They suggest benthic denitrification should have a much higher net fractionation factor due to the measured high $\delta^{15}NH_4^+$ that is presumably released from the sediments where benthic denitrification occurs. They propose this signal is due to fractionation during nitrification-denitrifcation loop in the sediments. If this high net fractionation factor is indeed correct on a global scale, higher BD : WCD ratios would be required to balance the nitrogen isotope budget because additional N_2 fixation would be needed to balance this "extra" ^{15}N-enriched nitrogen produced in the sediments where benthic denitrification occurs. However, ammonium efflux from the sediments is generally much higher on shallow shelves compared to deep ocean seafloor (Bohlen et al., 2012), suggesting that the global average fractionation of benthic denitrification is likely lower than these estimates (Lehmann et al., 2007). We test the sensitivity of this effect by running experiments with ε_{BD} set at 0, 2, and 4 ‰, while holding the lim WCD parameter constant at 32, which best represented $\delta^{15}NO_3^-$ observations in the suboxic zone.

The range of relative rates of BD : WCD required to closely reproduce observed global mean $\delta^{15}NO_3^-$ for our sensitivity experiments ($\varepsilon_{BD} = 0$–4 ‰) varied from 1.4–3.5. This represents a considerable range of benthic denitrification rates and suggests that a misrepresentation of this isotope effects can significantly bias the estimate for the BD : WCD ratio. The lack of water column $\delta^{15}NH_4^+$ measurements overlying sites of benthic denitrification, most notably in the deep ocean, make it difficult to constrain the global response at this time. We note our data-model analysis with the seafloor $\delta^{15}N$ database support these high estimates for the net fractionation factor of benthic denitrification ($\varepsilon_{BD} \geq 4$ ‰) in the Subarctic Ocean that contains many shallow shelves where benthic denitrification rates are high (Table 3 and Fig. 3).

4 Discussion

Our nitrogen isotope sensitivity experiments produce a large range of potential N_2 fixation and denitrification rates that vary by over a factor of 2 (Table 2, Fig. 2). We show that different nitrogen isotope parameters chosen for the isotope effects of water column and benthic N-loss significantly affect the estimates of the BD : WCD ratio needed to satisfy the global mean $\delta^{15}NO_3^-$ constraint. This is in general agreement with previous box model studies that also estimate a large range from 1–3.7 (Brandes and Devol, 2002; Deutsch et al., 2004; Altabet, 2007; Eugster and Gruber, 2012), when different isotope effects for denitrification were used in their respective models. These results show the importance of correctly modeling each isotope effect to simulate the balance of N_2 fixation and denitrification that determines the observed global mean $\delta^{15}NO_3^-$.

We create another global one-box $\delta^{15}NO_3^-$ model (called 0D in the following) that includes N_2 fixation, water column denitrification, and benthic denitrification to perform a more thorough sensitivity analysis of the key nitrogen isotope parameters. The 0D model is designed to calculate the required ratio of benthic to water column denitrification to maintain the observed global mean $\delta^{15}NO_3^-$ in a steady-state pre-industrial ocean. Its assumes that both the fixed marine nitrogen inventory as well as the inventory of $\delta^{15}NO_3^-$ are both in steady-state in the pre-industrial ocean. The 0D model then calculates the benthic to water column denitrification ratio required for different nitrogen isotope parameters chosen from previous model studies and the sensitivity experiments from this study (Table 2) using Eq. (A12).

The 0D model used here accurately reproduces the reported BD : WCD ratios of the various model configurations used in this study as well as previous studies despite the large range of model design and parameter selections (Table 4). This suggests our 0D model may be reliable to estimate the sensitivity of the different nitrogen isotope parameters in a steady-state scenario. It shows that the BD : WCD ratio needed to match global mean $\delta^{15}NO_3^-$ is very sensitive to the level of OMZ nitrate utilization and net fractionation factor chosen for benthic denitrification, as well as other parameters (Fig. 6). The range of uncertainty for these two effects can alone account for large range of estimates for benthic denitrification (100–280 Tg N yr^{-1}) from previous nitrogen isotope models (Brandes and Devol, 2002; Deutsch et al., 2004; Altabet, 2007; Eugster and Gruber, 2012).

The large uncertainty associated with the net fractionation factor of benthic denitrification adds further difficulties to constrain the BD : WCD ratio using global mean $\delta^{15}NO_3^-$. Our experiments show that increasing this factor from 0 to 4 ‰ requires almost triple the benthic denitrification rate needed to maintain the global mean $\delta^{15}NO_3^-$ at observed levels. Recent estimates suggest that the net fractionation factor may be even higher (4–8 ‰) due to fractionation within the nitrification-denitrification loop in the sediments (Granger et al., 2011; Alkhatib et al., 2012). If these high-end estimates are validated on a global scale, this could require larger BD : WCD ratios than our largest value simulated here (> 3.5). However, Lehmann et al. (2007) show that shallow regions have a higher net fractionation compared to deep ocean sites and the global average net fractionation is likely closer to 4 ‰. Our 0D experiments also show that no model configuration is able to support a global net fractionation factor for benthic denitrification greater than 6 ‰ and predict BD : WCD ratios in range of observational estimates (BD : WCD ≤ 4) (Fig. 6e).

The level of nitrate utilization in OMZs has a strong influence on the isotope effect of water column denitrification. It determines the $\delta^{15}NO_3^-$ value in water column denitrification zones that is consumed by denitrifiers. Figure 6c shows the range of BD : WCD ratios required for given $\delta^{15}NO_3^-$ signatures in the water column denitrification zones for all experiments. These idealized experiments using the parameter settings of lim WCD = 20, 26, and 32 (when $\varepsilon_{BD} = 0$) show that the different level of nitrate utilization, and its effect on $\delta^{15}NO_3^-$ in the water column denitrification zone, is causing the range of BD : WCD ratios from 0.8 to 1.4 in these experiments. This demonstrates that if this effect is not modeled accurately, it can lead to large biases of the estimates for denitrification.

For example, Brandes and Devol (2002) did not account for the locally high $\delta^{15}NO_3^-$ of water column denitrification zones in their one-box model (Fig. 6c). The $\delta^{15}NO_3^-$ removed during water column denitrification is thus much more ^{15}N-depleted compared to the other models that take into account nitrate utilization in the suboxic zone. This increases the isotope effect of water column denitrification in the Brandes and Devol (2002) model configuration and it thus needs more N_2 fixation to maintain global mean $\delta^{15}NO_3^-$, which is achieved by imposing a higher BD : WCD ratio. If they would have accounted for a more realistic suboxic zone $\delta^{15}NO_3^-$ signature in the range of the other model configurations, our 0D model suggests their estimate for BD : WCD would have been nearly a factor of 2 lower (Fig. 6c).

Our MOBI experiment #5 (lim WCD = 32, $\varepsilon_{BD} = 4$) is in general agreement with the final results of Brandes and Devol (2002) suggesting a relatively high rate of benthic denitrification, despite that the $\delta^{15}N$ model configuration for the isotope effects of water column and benthic denitrification is much different (Table 4). This suggests that even though the simple one-box model of Brandes and Devol (2002) was able to reach a similar result, it was due to different combination of isotope effects that are difficult to constrain in a one-box model. Whereas MOBI is directly comparable to $\delta^{15}N$ observations in regions where denitrification occurs in the water column and sediments, which allows better validation of the isotope effects.

The average level of nitrate utilization throughout the ocean's prominent suboxic zones remains difficult to assess. While studies in the ETNP and Arabian Sea OMZs do not typically show nitrate depleted below half of its expected value (Brandes et al., 1998; Voss et al., 2001), recent results from the ETSP suboxic zone show more than two-thirds of the expected nitrate was consumed (Ryabenko et al., 2012). However, they note large rates of benthic denitrification occurring within close proximity were likely contributing to this nitrate deficit. Furthermore, evidence from an eddy entraining suboxic water from the ETSP OMZ showed an even larger levels of nitrate utilization as it moved offshore (Altabet et al., 2012). These results suggests that average level of nitrate utilization in the global suboxic zones may be higher than off-shore observations from the Arabian Sea and ETNP included in Fig. 4. This would support lower ratios of BD : WCD in the global ocean (Altabet, 2007).

The 6-box model of Deutsch et al. (2004) accounts for local nitrate utilization with a designated suboxic box, but still estimates a higher BD : WCD ratio (2.69) compared to the results from our MOBI experiment in which the fractionation factor for benthic denitrification was also set to 0 ‰ (BD : WCD = 1.4). The most significant difference between the Deutsch et al. (2004) and the other model configurations is the isotope effect of N_2 fixation. Deutsch et al. (2004) choose a $\delta^{15}N_{Nfix}$ signature of 0 ‰, while all other models selected between −1 and −1.5 ‰. If the Deutsch et al. (2004) study would have chosen the same value as here ($\delta^{15}N_{Nfix} = -1.5$ ‰), our 0D model suggests this would decrease their estimated BD : WCD ratio from 2.69 to 1.83, which would then be more consistent with the results from MOBI. This shows that even small differences (< 2 ‰) for the isotope effect of N_2 fixation can alter the ratio of BD : WCD by 30 % or even more depending on the model configuration used (Fig. 6d).

The MOBI experiments that best reproduce seafloor $\delta^{15}N$ observations are experiments #4 and #5 (lim WCD = 32, $\varepsilon_{BD} = 2$ and 4) (Table 2). They predict a range of rates for N_2 fixation, water column denitrification, and benthic denitrification between

225–342, 76, and 149–267 Tg N yr^{-1}, respectively. These experiments produce a large range of BD : WCD ratios from 2 to 3.5 and highlight the high sensitivity of the BD : WCD ratio to the net fractionation factor of benthic denitrification. Although the average level of nitrate utilization in the suboxic zones is also uncertain, our experiments using lim WCD = 32 best represented observations from the ETNP and Arabian Sea. Assuming this range for nitrogen isotope parameters, our model estimates a potential range for BD : WCD of 2.0–3.5. This range suggests that rates of N_2 fixation, water column denitrification, and benthic denitrification are between 195–345, 65–75, and 130–270 Tg N yr^{-1}, respectively, assuming a balanced fixed nitrogen budget. This model result estimates that the residence time of oceanic fixed-N is in the range of 1500 to 3000 yr.

Our model experiments are in general agreement with a recent 3-D inverse model that included nitrogen isotopes to constrain marine denitrification rates (DeVries et al., 2012). They similarly show a high sensitivity to the NO_3^- utilization in the suboxic zone and fractionation factor assumed for benthic denitrification. However, they estimate lower ratios of BD : WCD from 1.3–2.3 compared to our results with MOBI. The main reasons for this discrepancy is likely that DeVries et al. (2012) assumed slightly higher level of nitrate utilization in the suboxic zones and tested lower values for the fractionation factor of benthic denitrification (0 to 3 ‰) compared to our study, both of which will require lower BD : WCD ratios. Whereas our high-end estimate for BD : WCD = 3.5 is due to using a benthic denitrification fractionation factor of 4 ‰. The high sensitivity to these parameters emphasize the need to better understand and quantify them in future studies.

5 Conclusions

Our study uses water column $\delta^{15}NO_3^-$ and seafloor $\delta^{15}N$ observations to constrain the rates of N_2 fixation, water column denitrification, and benthic denitrification in the global ocean. The uncertainty associated with isotope effects of denitrification in the water column and sediments makes it difficult to constrain N_2 fixation and total denitrification rates. Previous box model studies using δ^{15}N have estimated a large range for the ratio of BD : WCD from 1 to 3.7 (Brandes and Devol, 2002; Deutsch et al., 2004; Altabet, 2007; Eugster and Gruber, 2012). Here we used a set of experiments with a global coupled three-dimensional circulation-biogeochemistry-isotope model (MOBI) and a one-box model to show that nitrate utilization in the suboxic zone and the net fractionation factor of benthic denitrification, both of which are not well constrained by observations, can lead to rates of benthic denitrification that vary by over a factor of 2 if not modeled correctly.

With our global coupled three-dimensional model, we are able to compare δ^{15}N observations in the water column and seafloor in the regions where denitrification occurs to constrain the nitrogen isotope parameters in the model. This highlights the importance of using models that can resolve all of the locally important nitrogen isotope effects that affect δ^{15}N in denitrification zones. The model experiments that best reproduce δ^{15}N observations in the water column and sediments estimate the rates of N_2 fixation, water column denitrification, and benthic denitrification in the range 195–345, 65–75, and 130–270 Tg N yr^{-1}, respectively, assuming a balanced fixed-N budget in the pre-industrial ocean. Although uncertainties still exist, this model result suggests previous estimates of N_2 fixation have been underestimated and the residence time for oceanic fixed nitrogen is between 1500 and 3000 yr.

Appendix A

Nitrogen isotope model description

A1 Fractionation equation

Fractionation is calculated using kinetic fractionation (Mariotti et al., 1981):

$$\frac{{}^{15}\mathrm{N}_{\mathrm{pro}}}{{}^{14}\mathrm{N}_{\mathrm{pro}}} = \alpha \frac{{}^{15}\mathrm{N}_{\mathrm{sub}}}{{}^{14}\mathrm{N}_{\mathrm{sub}}} \tag{A1}$$

where α is the kinetic fractionation factor associated with the process and the $\mathrm{N}_{\mathrm{pro}}$ and $\mathrm{N}_{\mathrm{sub}}$ refer to the nitrogen of the product and substrate of the reaction, respectively. In the model, we include ^{15}N as the prognostic variable instead of the ratio $^{15}\mathrm{N}/^{14}\mathrm{N}$. The ^{15}N equations are embedded within the marine ecosystem model that calculates total N ($^{\mathrm{T}}\mathrm{N} = {}^{15}\mathrm{N} + {}^{14}\mathrm{N}$). Solving Eq. (A1) for $^{15}\mathrm{N}_{\mathrm{pro}}$ with respect to $^{\mathrm{T}}\mathrm{N}_{\mathrm{pro}}$ yields

$${}^{15}\mathrm{N}_{\mathrm{pro}} = \frac{\alpha R_{\mathrm{sub}}}{1 + \alpha R_{\mathrm{sub}}} {}^{\mathrm{T}}\mathrm{N}_{\mathrm{pro}}. \tag{A2}$$

where R_{sub} is the isotopic ratio $^{15}\mathrm{N}/^{14}\mathrm{N}$ of the substrate of the reaction.

This equation can be equivalently expressed in the commonly used delta ("δ") notation by applying the relation (Mariotti et al., 1981):

$$\alpha = 1 - \varepsilon/1000 \tag{A3}$$

which gives positive values for ε with this definition. Equation (A2) then becomes

$${}^{15}\mathrm{N}_{\mathrm{pro}} = \frac{\beta}{1 + \beta} {}^{\mathrm{T}}\mathrm{N}_{\mathrm{pro}} \tag{A4}$$

where $\beta = R_{\text{sub}}(1-\varepsilon/1000)$ (Giraud et al., 2000), which is the nitrogen isotope equation coded into the marine ecosystem-biogeochemistry model. Note we use a R_{std} value of 1 so that ^{14}N and ^{15}N have concentrations of the same order of magnitude. This reduces the impact of numerical noise caused by the advection scheme on the δ^{15}N value. If the atmospheric N_2 ratio is used ($R_{\text{std}} = 0.0036765$), the ^{15}N concentration would be over two orders of magnitude smaller and be more susceptible to numerical noise, which produces erroneous δ^{15}N values. In the polar oceans (> 80° N/S) where numerical noise is the highest, some model grid points still contain erroneous isotope values and are discarded in the statistical analysis.

A2 Coupled model equations

The fractionation equation used for NO_3^- consumption during phytoplankton uptake and water column denitrification follows Eq. (A4) where $\beta = R_{\text{sub}}[1-\varepsilon\cdot(1-u)/u\cdot\ln(1-u)/1000]$ and u is the fraction of available total nitrate consumed during each time-step. This fractionation equation is used to ensure that if a significant portion of the nitrate pool is consumed in one time-step, mass balance of the different nitrogen isotope species is conserved. In the experiments here, we artificially limit water column denitrification at high enough nitrate concentrations (26–32 µM) so this term $[(1-u)/u\cdot\ln(1-u)]$ has a negligible effect for water column denitrification in this study. Since zooplankton excretion and benthic denitrification are parameterized in the model, the instantaneous fractionation equation is used (Eq. A4) with a given fractionation factor to mimic the net fractionation that occurs during the integrated reaction.

The full set of time-dependent equations for ^{15}N that are embedded into the marine ecosystem biogeochemical model are as follows:

$$\frac{\partial\, {}^{15}\mathrm{NO_3^-}}{\partial t} = \left({}^{\mathrm{T}}R_{\mathrm{D}}\mu_{\mathrm{D}}D + \frac{\beta_{\mathrm{excr}}}{1+\beta_{\mathrm{excr}}}\mu_{Z_0}Z + {}^{\mathrm{T}}R_{P_{\mathrm{O}}}\mu_{P_{\mathrm{O}}}P_{\mathrm{O}} - \frac{\beta_{\mathrm{assim}}}{1+\beta_{\mathrm{assim}}}J_{\mathrm{O}}P_{\mathrm{O}} \right.$$
$$\left. - \frac{\beta_{\mathrm{assim}}}{1+\beta_{\mathrm{assim}}}u_{\mathrm{NO_3^-}}J_{\mathrm{D}}P_{\mathrm{D}}\right)$$
$$\times \left[1 - \frac{\beta_{\mathrm{WCD}}}{1+\beta_{\mathrm{WCD}}}0.8r_{\mathrm{O:N}}\rho_{\mathrm{sox}}^{\mathrm{NO_3^-}}L_{\mathrm{WCD}}\right] - \frac{\beta_{\mathrm{BD}}}{1+\beta_{\mathrm{BD}}}\alpha_{\mathrm{BD}}\mathrm{BD}\cdot L_{\mathrm{BD}} \qquad \text{(A5)}$$

$$\frac{\partial\, {}^{15}\mathrm{N}{-}P_{\mathrm{O}}}{\partial t} = \frac{\beta_{\mathrm{assim}}}{1+\beta_{\mathrm{assim}}}J_{\mathrm{O}}P_{\mathrm{O}} - {}^{\mathrm{T}}R_{P_{\mathrm{O}}}\mu_{P_{\mathrm{O}}}P_{\mathrm{O}} - {}^{\mathrm{T}}R_{P_{\mathrm{O}}}G(P_{\mathrm{O}})Z - {}^{\mathrm{T}}R_{P_{\mathrm{O}}}v_{P_{\mathrm{O}}}P_G^2 \qquad \text{(A6)}$$

$$\frac{\partial\, {}^{15}\mathrm{N}{-}P_{\mathrm{D}}}{\partial t} = \left(\frac{\beta_{\mathrm{assim}}}{1+\beta_{\mathrm{assim}}}u_{\mathrm{NO_3^-}} + \frac{\beta_{\mathrm{Nfix}}}{1+\beta_{\mathrm{Nfix}}}(1-u_{\mathrm{NO_3^-}})\right)J_{\mathrm{D}}P_{\mathrm{D}}$$
$$- {}^{\mathrm{T}}R_{P_{\mathrm{D}}}\mu_{P_{\mathrm{D}}}P_{\mathrm{D}} - {}^{\mathrm{T}}R_{P_{\mathrm{D}}}G(P_{\mathrm{D}})Z - {}^{\mathrm{T}}R_{P_{\mathrm{D}}}v_{P_{\mathrm{D}}}P_{\mathrm{D}}^2 \qquad \text{(A7)}$$

$$\frac{\partial\, {}^{15}\mathrm{N}{-}Z}{\partial t} = \gamma\left[{}^{\mathrm{T}}R_{P_{\mathrm{O}}}G(P_{\mathrm{O}}) + {}^{\mathrm{T}}R_{\mathrm{P}}G(P_{\mathrm{D}})\right]Z - \frac{\beta_{\mathrm{excr}}}{1+\beta_{\mathrm{excr}}}\mu_{Z_0}Z - {}^{\mathrm{T}}R_Z v_Z Z^2 \qquad \text{(A8)}$$

$$\frac{\partial\, {}^{15}\mathrm{N}{-}D}{\partial t} = (1-\gamma)\left[{}^{\mathrm{T}}R_{P_{\mathrm{O}}}G(P_{\mathrm{O}}) + {}^{\mathrm{T}}R_{P_{\mathrm{D}}}G(P_{\mathrm{D}})\right]Z - {}^{\mathrm{T}}R_{\mathrm{D}}\mu_{\mathrm{D}}D + {}^{\mathrm{T}}R_{P_{\mathrm{O}}}v_{P_{\mathrm{O}}}P_O^2$$
$$+ {}^{\mathrm{T}}R_{P_{\mathrm{D}}}v_{P_{\mathrm{D}}}P_{\mathrm{D}}^2 + {}^{\mathrm{T}}R_Z v_Z Z^2 - {}^{\mathrm{T}}R_{\mathrm{D}}w_{\mathrm{D}}\frac{\partial D}{\partial z} \qquad \text{(A9)}$$

where ${}^{\mathrm{T}}R_X = {}^{15}\mathrm{N}_X/({}^{15}\mathrm{N}_X + {}^{14}\mathrm{N}_X)$. Here it suffices to note that the equations for total nitrogen (^{14}N + ^{15}N) are identical to the ones of ^{15}N, except that ${}^{\mathrm{T}}R_X = \beta_X/(1+\beta_X) = 1$ in the total nitrogen equations. The parameter list is given in Table A1.

A3 One-box 0D$\delta^{15}NO_3^-$ Model

The one-box δ^{15}N 0D model assumes the fixed nitrogen inventory and the nitrogen isotope inventory are both in steady-state. This yields the equations:

$$\mathrm{Nfix} = \mathrm{WCD} + \mathrm{BD} \tag{A10}$$

$$\mathrm{Nfix}\cdot\left(\frac{\beta}{1+\beta}\right)_{\mathrm{Nfix}} = \mathrm{WCD}\cdot\left(\frac{\beta}{1+\beta}\right)_{\mathrm{WCD}} + \mathrm{BD}\cdot\left(\frac{\beta}{1+\beta}\right)_{\mathrm{BD}} \tag{A11}$$

where $\beta = \alpha \cdot R_{\mathrm{sub}} = R_{\mathrm{sub}}(1 - \varepsilon/1000)$, consistent with Eq. (A4). Solving for benthic to water column denitrification ratio yields

$$\frac{\mathrm{BD}}{\mathrm{WCD}} = \frac{\left(\frac{\beta}{1+\beta}\right)_{\mathrm{Nfix}} - \left(\frac{\beta}{1+\beta}\right)_{\mathrm{WCD}}}{\left(\frac{\beta}{1+\beta}\right)_{\mathrm{BD}} - \left(\frac{\beta}{1+\beta}\right)_{\mathrm{Nfix}}}. \tag{A12}$$

These results are displayed in Table 4 and Fig. 6.

Appendix B

Marine ecosystem-biogeochemistry model description

This appendix provides a description of the parameters used in the full set of time-dependent equations in the marine ecosystem model. It suffices to note that the equations for total nitrogen (^{14}N + ^{15}N) ecosystem variables are identical to the ones of ^{15}N if $R_X = \beta_X/(1+\beta_X) = 1$, which are located in Appendix A.

The function J_O provides the growth rate of non-diazotrophic "ordinary" phytoplankton, determined from irradiance (I), NO_3^- and PO_4^{3-},

$$J_O(I, NO_3^-, PO_4^{3-}) = \min(J_{OI}, J_{O\max}u_N, J_{O\max}u_P) \tag{B1}$$

The maximum growth rate is dependent only on temperature (T):

$$J_{O\,\mathrm{max}} = a \cdot \exp(T/T_\mathrm{b}) \tag{B2}$$

such that growth rates increase by a factor of ten over the temperature range of −2 to 34 °C. We use $a = 0.35\,\mathrm{d}^{-1}$ for the maximum growth rate at 0 °C which was determined to optimize surface nutrient concentrations. Under nutrient-replete conditions, the light-limited growth rate J_{OI} is calculated according to:

$$J_{OI} = \frac{J_{O\,\mathrm{max}}\alpha I}{\left[J^2_{O\,\mathrm{max}} + (\alpha I)^2\right]^{1/2}} \tag{B3}$$

where α is the initial slope of the photosynthesis vs. irradiance (P-I) curve. The calculation of the photosynthetically active shortwave radiation I and the method of averaging equation (C-3) over one day is outlined in (Schmittner et al., 2005). This version also includes in the correction for the error in the calculation of light limitation in previous versions (Schmittner et al., 2008b). Nutrient limitation is represented by the product of $J_{O\,\mathrm{max}}$ and the nutrient uptake rates, $u_\mathrm{N} = \mathrm{NO}_3^-/(k_\mathrm{N} + \mathrm{NO}_3^-)$ and $u_\mathrm{P} = \mathrm{PO}_4^{3-}/(k_\mathrm{P} + \mathrm{PO}_4^{3-})$, with $k_\mathrm{P} = k_\mathrm{N} r_\mathrm{P:N}$ providing the respective nutrient uptake rates.

Diazotrophs grow according to the same principles as the ordinary phytoplankton class, but are disadvantaged in nitrate-bearing waters by a lower maximum growth rate, $J_{D\,\mathrm{max}}$, which is set to zero below 15 °C:

$$J_{D\,\mathrm{max}} = c_\mathrm{D} \cdot \mathrm{FeLim} \cdot a \cdot \exp(T/T_\mathrm{b}) \tag{B4}$$

The coefficient c_D handicaps diazotrophs by dampening the increase of their maximal growth rate versus that of the general phytoplankton class with rising temperature. We use $c_\mathrm{D} = 0.13$, such that the growth rate of diazotrophs is 13 % that of ordinary phytoplankton. This handicap is further decreased by the Fe limitation parameter, which is scaled between 0–1 by multiplying a monthly climatology of aeolian dust deposition

(Mahowald et al., 2005b, 2006, 2009) by a constant factor and setting the maximum value to 1 (Somes et al., 2010a). However, diazotrophs have an advantage in that their growth rate is not limited by NO_3^- concentrations:

$$J_{\mathrm{D}}(I,\mathrm{PO_4}) = \min(J_{DI}, J_{\mathrm{D\,max}} u_{\mathrm{P}}) \tag{B5}$$

although they do take up NO_3^- if it is available (see term 5 in the right hand side of Eq. A10). The N : P of model diazotrophs is set to 40 : 1.

The first order mortality rate of phytoplankton is linearly dependent on their concentration, P_{O}. DOM and the microbial loop are folded into a single fast-remineralization process, which is the product of P_{O} and the temperature dependent term

$$\mu_{\mathrm{P}} = \mu_{\mathrm{PO}} \exp(T/T_{\mathrm{b}}). \tag{B6}$$

Diazotrophs also die at a linear rate which is included into this fast-remineralization process.

The grazing of ordinary phytoplankton and diazotrophs by zooplankton remains unchanged from Schmittner et al. (2005) as follows:

$$G(P) = \frac{g\varpi P^2}{g + \varpi P^2} \tag{B7}$$

where g is grazing rate, ϖ is prey-capture rate, and P is phytoplankton concentration (Table A1). Note prey-capture rate is reduced for diazotrophs relative to ordinary phytoplankton in these experiments (Table 1).

Detritus is generated from sloppy zooplankton feeding and mortality among the three classes of plankton, and is the only component of the ecosystem model to sink. It does so at a speed of

$$w_{\mathrm{D}} = \left\{ \begin{array}{c} w_{D0} + m_w z, z \leq 1000\,\mathrm{m} \\ w_{D0} + m_w 1000\,\mathrm{m}, z > 1000\,\mathrm{m} \end{array} \right\}, \tag{B8}$$

Title Page
Abstract | Introduction
Conclusions | References
Tables | Figures
◀| |▶
◀ ▶
Back | Close
Full Screen / Esc
Printer-friendly Version
Interactive Discussion

increasing linearly with depth z from $w_{D0} = 7\,\mathrm{m\,d^{-1}}$ at the surface to $40\,\mathrm{m\,d^{-1}}$ at 1 km depth and constant below that, consistent with observations (Berelson, 2001). The remineralization rate of detritus is temperature dependent and decreases by a factor of 2 in suboxic waters, as O_2 decreases from 10 µM to 0 µM:

$$\mu_D = \mu_{DO}\exp(T/T_b)[0.75 + 0.25\tanh(O_2 - 6)] \tag{B9}$$

Remineralization transforms the N and P content of detritus to NO_3^- and PO_4^{3-}. Photosynthesis produces oxygen, while respiration consumes oxygen, at rates equal to the consumption and remineralization rates of PO_4, respectively, multiplied by the constant ratio $R_{O:P}$. Dissolved oxygen exchanges with the atmosphere in the surface layer (F_{sfc}) according to the OCMIP protocol.

Oxygen consumption in suboxic waters ($O_2 < \sim 5\,\mu M$) is inhibited, according to

$$r_{sox}^{O_2} = 0.5[\tanh(O_2 - 5) + 1] \tag{B10}$$

but is replaced by the oxygen-equivalent oxidation of nitrate,

$$r_{sox}^{NO_3} = 0.5[1 - \tanh(O_2 - 5)]. \tag{B11}$$

Denitrification consumes nitrate at a rate of 80 % of the oxygen equivalent rate, as NO_3 is a more efficient oxidant on a mol per mol basis (i.e. one mol of NO_3 can accept 5 e^- while 1 mol of O_2 can accept only 4 e^-).

We include the benthic N-loss scheme of Bohlen et al. (2012), which parameterizes benthic N-loss based on the labile carbon flux (F_c) into the sediments and bottom water oxygen and nitrate:

$$\mathrm{BenDeni} = \left(0.09782 + 0.22944 \times 0.9811^{\mathrm{bwO_2} - \mathrm{NO_3^-}}\right) \times RR_{POC} \tag{B12}$$

BenDeni is the rate at which nitrate is removed from the bottom water. We assume that the rain rate of carbon into the sediments occurs at a ratio of $R_{C:N} = 6.625$ of the nitrogen in the sinking organic detritus.

Since the continental shelves are not well resolved in the model, we use an additional sub-grid scale parameterization for them. The portion of each bottom ocean grid box that is deeper than the real sea floor is calculated at each location from high resolution (1/5°) bathymetry. The rain rate of carbon that is included in the benthic N-loss function in this shelf parameterization is the amount of particulate organic carbon that sinks into the portion of the grid box covered by a shallower continental shelf. In the model, ~ 30 % of the benthic denitrification occurs within this shelf parameterization. The remaining particulate organic matter continues to sink to greater depths. The coarse-resolution physical circulation model's inability to fully resolve coastal systems generally underestimates primary production and sinking carbon fluxes on these continental shelves, which results in too low benthic N-loss rates there. To account for this deficiency, we arbitrarily multiply the benthic denitrification transfer function by a coefficient (α_{BD}). This parameter is tuned to set the global deep ocean $\delta^{15}NO_3^-$ in the model to ~ 5 ‰ for each experiment. Figure 2 shows the spatial distribution of benthic denitrification.

Acknowledgements. Funding of this work was provided by the SFB754 project from the German Research Foundation.

The service charges for this open access publication
have been covered by a Research Centre of the
Helmholtz Association.

References

Alkhatib, M., Lehmann, M. F., and del Giorgio, P. A.: The nitrogen isotope effect of benthic remineralization-nitrification-denitrification coupling in an estuarine environment, Biogeosciences, 9, 1633–1646, doi:10.5194/bg-9-1633-2012, 2012.

Altabet, M. A.: Constraints on oceanic N balance/imbalance from sedimentary ^{15}N records, Biogeosciences, 4, 75–86, doi:10.5194/bg-4-75-2007, 2007.

Title Page
Abstract | Introduction
Conclusions | References
Tables | Figures
◀▮ | ▶▮
◀ | ▶
Back | Close
Full Screen / Esc
Printer-friendly Version
Interactive Discussion

Altabet, M. A., Francois, R., Murray, D. W., and Prell, W. L.: Climate-related variations in denitrification in the arabian sea from sediment $^{15}N/^{14}N$ ratios, Nature, 373, 506–509, 1995.

Altabet, M. A., Ryabenko, E., Stramma, L., Wallace, D. W. R., Frank, M., Grasse, P., and Lavik, G.: An eddy-stimulated hotspot for fixed nitrogen-loss from the Peru oxygen minimum zone, Biogeosciences, 9, 4897–4908, doi:10.5194/bg-9-4897-2012, 2012.

Antonov, J. I., Seidov, D., Boyer, T. P., Locarnini, R. A., Mishonov, A. V., Garcia, H. E., Baranova, O. K., Zweng, M. M., and Johnson, D. R.: World ocean atlas 2009, volume 2: Salinity, in: NOAA Atlas Nesdis 69, edited by: Levitus, S., US Government Printing Office, Washington, DC, 184, 2010.

Aumont, O., Maier-Reimer, E., Blain, S., and Monfray, P.: An ecosystem model of the global ocean including Fe, Si, P colimitations, Global Biogeochem. Cy., 17, 1060, doi:10.1029/2001gb001745, 2003.

Berelson, W. M.: Particle settling rates increase with depth in the ocean, Deep-Sea Res. Pt. II, 49, 237–251, doi:10.1016/S0967-0645(01)00102-3, 2001.

Bianchi, D., Dunne, J. P., Sarmiento, J. L., and Galbraith, E. D.: Data-based estimates of suboxia, denitrification, and N_2O production in the ocean and their sensitivities to dissolved O_2, Global Biogeochem. Cy., 26, GB2009, doi:10.1029/2011gb004209, 2012.

Bohlen, L., Dale, A. W., and Wallmann, K.: Simple transfer functions for calculating benthic fixed nitrogen losses and C : N : P regeneration ratios in global biogeochemical models, Global Biogeochem. Cy., 26, GB3029, doi:10.1029/2011gb004198, 2012.

Brandes, J. A. and Devol, A. H.: A global marine-fixed nitrogen isotopic budget: implications for holocene nitrogen cycling, Global Biogeochem. Cy., 16, 1120, doi:10.1029/2001GB001856, 2002.

Brandes, J. A., Devol, A. H., Yoshinari, T., Jayakumar, D. A., and Naqvi, S. W. A.: Isotopic composition of nitrate in the central Arabian Sea and eastern tropical North Pacific: a tracer for mixing and nitrogen cycles, Limn. Ocean., 43, 1680–1689, 1998.

Bulow, S. E., Rich, J. J., Naik, H. S., Pratihary, A. K., and Ward, B. B.: Denitrification exceeds anammox as a nitrogen loss pathway in the arabian sea oxygen minimum zone, Deep-Sea Res. Pt. I, 57, 384–393, 2010.

Cline, J. D. and Kaplan, I. R.: Isotopic fractionation of dissolved nitrate during denitrification in the eastern tropical North Pacific Ocean, Mar. Chem., 3, 271–299, 1975.

Codispoti, L. A.: An oceanic fixed nitrogen sink exceeding 400 Tg N a^{-1} vs the concept of homeostasis in the fixed-nitrogen inventory, Biogeosciences, 4, 233–253, doi:10.5194/bg-4-233-2007, 2007.

Codispoti, L. A., Brandes, J. A., Christensen, J. P., Devol, A. H., Naqvi, S. W. A., Paerl, H. W., and Yoshinari, T.: The oceanic fixed nitrogen and nitrous oxide budgets: moving targets as we enter the anthropocene?, Sci. Mar., 65, 85–105, 2001.

Deutsch, C., Sigman, D. M., Thunell, R. C., Meckler, A. N., and Haug, G. H.: Isotopic constraints on glacial/interglacial changes in the oceanic nitrogen budget, Global Biogeochem. Cy., 18, GB4012, doi:10.1029/2003gb002189, 2004.

Deutsch, C., Sarmiento, J. L., Sigman, D. M., Gruber, N., and Dunne, J. P.: Spatial coupling of nitrogen inputs and losses in the ocean, Nature, 445, 163–167, doi:10.1038/nature05392, 2007.

DeVries, T., Deutsch, C., Rafter, P. A., and Primeau, F.: Marine denitrification rates determined from a global 3-dimensional inverse model, Biogeosciences Discuss., 9, 14013–14052, doi:10.5194/bgd-9-14013-2012, 2012.

Duce, R. A., LaRoche, J., Altieri, K., Arrigo, K. R., Baker, A. R., Capone, D. G., Cornell, S., Dentener, F., Galloway, J., Ganeshram, R. S., Geider, R. J., Jickells, T., Kuypers, M. M., Langlois, R., Liss, P. S., Liu, S. M., Middelburg, J. J., Moore, C. M., Nickovic, S., Oschlies, A., Pedersen, T., Prospero, J., Schlitzer, R., Seitzinger, S., Sorensen, L. L., Uematsu, M., Ulloa, O., Voss, M., Ward, B., and Zamora, L.: Impacts of atmospheric anthropogenic nitrogen on the open ocean, Science, 320, 893–897, doi:10.1126/science.1150369, 2008.

Eby, M., Zickfeld, K., Montenegro, A., Archer, D., Meissner, K. J., and Weaver, A. J.: Lifetime of anthropogenic climate change: millennial time scales of potential co2 and surface temperature perturbations, J. Climate, 22, 2501–2511, doi:10.1175/2008jcli2554.1, 2009.

Eugster, O. and Gruber, N.: A probabilistic estimate of global marine n-fixation and denitrification, Global Biogeochem. Cy., 26, GB4013, doi:10.1029/2012gb004300, 2012.

Falkowski, P. G.: Evolution of the nitrogen cycle and its influence on the biological sequestration of CO_2 in the ocean, Nature, 387, 272–275, 1997.

Foster, R. A., Kuypers, M. M. M., Vagner, T., Paerl, R. W., Musat, N., and Zehr, J. P.: Nitrogen fixation and transfer in open ocean diatom-cyanobacterial symbioses, ISME J., 5, 1484–1493, 2011.

Galbraith, E. D., Gnanadesikan, A., Dunne, J. P., and Hiscock, M. R.: Regional impacts of iron-light colimitation in a global biogeochemical model, Biogeosciences, 7, 1043–1064, doi:10.5194/bg-7-1043-2010, 2010.

Galloway, J. N., Dentener, F. J., Capone, D. G., Boyer, E. W., Howarth, R. W., Seitzinger, S. P., Asner, G. P., Cleveland, C. C., Green, P. A., Holland, E. A., Karl, D. M., Michaels, A. F., Porter, J. H., Townsend, A. R., and Vöosmarty, C. J.: Nitrogen cycles: past, present, and future, Biogeochemistry, 70, 153–226, doi:10.1007/s10533-004-0370-0, 2004.

Garcia, H. E., Locarnini, R. A., Boyer, T. P., Antonov, J. I., Baranov, O. K., Zweng, M. M., and Johnson, D. R.: World ocean atlas 2009, volume 3: dissolved oxygen, apparent oxygen utilization, and oxygen saturation, in: NOAA Atlas Nesdis 70, edited by: Levitus, S., US Government Printing Office, Washington, DC, 344, 2010a.

Garcia, H. E., Locarnini, R. A., Boyer, T. P., Antonov, J. I., Zweng, M. M., Baranov, O. K., and Johnson, D. R.: World ocean atlas 2009, volume 4: nutrients (phosphate, nitrate, silicate), in: NOAA Atlas Nesdis 71, edited by: Levitus, S., US Government Printing Office, Washington, DC, 398, 2010b.

Gent, P. R. and McWilliams, J. C.: Isopycnal mixing in ocean circulation models, J. Phys. Oceanogr., 20, 150–155, doi:10.1175/1520-0485(1990)020<0150:IMIOCM>2.0.CO;2, 1990.

Giraud, X., Bertrand, P., Garc, on, V., and Dadou, I.: Modeling delta15n evolution: first palaeoceanographic applications in a coastal upwelling system, J. Mar. Res., 58, 609–630, 2000.

Gnanadesikan, A., Dunne, J. P., and John, J.: Understanding why the volume of suboxic waters does not increase over centuries of global warming in an Earth System Model, Biogeosciences, 9, 1159–1172, doi:10.5194/bg-9-1159-2012, 2012.

Granger, J., Prokopenko, M. G., Sigman, D. M., Mordy, C. W., Morse, Z. M., Morales, L. V., Sambrotto, R. N., and Plessen, B.: Coupled nitrification-denitrification in sediment of the eastern bering sea shelf leads to ^{15}N enrichment of fixed N in shelf waters, J. Geophys. Res., 116, C11006, doi:10.1029/2010jc006751, 2011.

Großkopf, T., Mohr, W., Baustian, T., Schunck, H., Gill, D., Kuypers, M. M. M., Lavik, G., Schmitz, R. A., Wallace, D. W. R., and LaRoche, J.: Doubling of marine dinitrogen-fixation rates based on direct measurements, Nature, 488, 361–364, http://www.nature.com/nature/journal/v488/n7411/abs/nature11338.html#supplementary-information, 2012.

Gruber, N.: The dynamics of the marine nitrogen cycle and its influence on atmospheric CO_2 variations, in: The Ocean Carbon Cycle and Climate, 4th edn., edited by: Follows, M. and Oguz, T., Nato science series, Kluwer Academics, Dordrecht, 97–148, 2004.

Gruber, N.: Chapter 1 – the marine nitrogen cycle: overview and challenges, in: Nitrogen in the Marine Environment, 2nd edn., Academic Press, San Diego, 1–50, 2008.

Gruber, N. and Sarmiento, J. L.: Global patterns of marine nitrogen fixation and denitrification, Global Biogeochem. Cy., 11, 235–266, doi:10.1029/97gb00077, 1997.

Holl, C. M. and Montoya, J. P.: Interactions between nitrate uptake and nitrogen fixation in continuous cultures of the marine diazotroph *trichodesmium* (cyanobacteria), J. Phycol., 41, 1178–1183, doi:10.1111/j.1529-8817.2005.00146.x, 2005.

Kalnay, E., Kanamitsu, M., Kistler, R., Collins, W., Deaven, D., Gandin, L., Iredell, M., Saha, S., White, G., Woollen, J., Zhu, Y., Leetmaa, A., Reynolds, R., Chelliah, M., Ebisuzaki, W., Higgins, W., Janowiak, J., Mo, K. C., Ropelewski, C., Wang, J., Jenne, R., and Joseph, D.: The ncep/ncar 40-year reanalysis project, B. Am. Meteorol. Soc., 77, 437–471, doi:10.1175/1520-0477(1996)077<0437:tnyrp>2.0.co;2, 1996.

Karl, D., Michaels, A., Bergman, B., Capone, D., Carpenter, E., Letelier, R., Lipshultz, F., Paerl, H., Sigman, D., and Stal, L.: Dinitrogen fixation in the world's oceans, Biogeochemistry, 57/58, 47–98, 2002.

Klausmeier, C. A., Litchman, E., Daufresne, T., and Levin, S. A.: Optimal nitrogen-to-phosphorus stoichiometry of phytoplankton, Nature, 429, 171–174, doi:10.1038/nature02454, 2004.

Kuypers, M. M. M., Sliekers, A. O., Lavik, G., Schmid, M., Jorgensen, B. B., Kuenen, J. G., Sinninghe Damste, J. S., Strous, M., and Jetten, M. S. M.: Anaerobic ammonium oxidation by anammox bacteria in the black sea, Nature, 422, 608–611, 2003.

Kuypers, M. M. M., Lavik, G., Woebken, D., Schmid, M., Fuchs, B. M., Amann, R., Jørgensen, B. B., and Jetten, M. S. M.: Massive nitrogen loss from the benguela upwelling system through anaerobic ammonium oxidation, P. Natl. Acad. Sci. USA, 102, 6478–6483, doi:10.1073/pnas.0502088102, 2005.

Lam, P., Lavik, G., Jensen, M. M., van de Vossenberg, J., Schmid, M., Woebken, D., Gutiérrez, D., Amann, R., Jetten, M. S. M., and Kuypers, M. M. M.: Revising the nitrogen cycle in the peruvian oxygen minimum zone, P. Natl. Acad. Sci. USA, 106, 4752–4757, doi:10.1073/pnas.0812444106, 2009.

Large, W. G., Danabasoglu, G., McWilliams, J. C., Gent, P. R., and Bryan, F. O.: Equatorial circulation of a global ocean climate model with anisotropic horizontal viscosity, J. Phys. Oceanogr., 31, 518–536, doi:10.1175/1520-0485(2001)031<0518:ECOAGO>2.0.CO;2, 2001.

Le Quéré, C. L., Harrison, S. P., Colin Prentice, I., Buitenhuis, E. T., Aumont, O., Bopp, L., Claustre, H., Cotrim Da Cunha, L., Geider, R., Giraud, X., Klaas, C., Kohfeld, K. E., Legendre, L., Manizza, M., Platt, T., Rivkin, R. B., Sathyendranath, S., Uitz, J., Watson, A. J., and Wolf-Gladrow, D.: Ecosystem dynamics based on plankton functional types for global ocean biogeochemistry models, Global Change Biol., 11, 2016–2040, doi:10.1111/j.1365-2486.2005.1004.x, 2005.

Lehmann, M. F., Sigman, D. M., and Berelson, W. M.: Coupling the ^{15}N/^{14}N and ^{18}O/^{16}O of nitrate as a constraint on benthic nitrogen cycling, Mar. Chem., 88, 1–20, 2004.

Lehmann, M. F., Sigman, D. M., McCorkle, D. C., Granger, J., Hoffmann, S., Cane, G., and Brunelle, B. G.: The distribution of nitrate ^{15}N/^{14}N in marine sediments and the impact of benthic nitrogen loss on the isotopic composition of oceanic nitrate, Geochim. Cosmochim. Ac., 71, 5384–5404, 2007.

Letelier, R. M. and Karl, D. M.: Trichodesmium spp. physiology and nutrient fluxes in the north pacific subtropical gyre, Aquat. Microb. Ecol., 15, 265–276, doi:10.3354/ame015265, 1998.

Locarnini, R. A., Mishonov, A. V., Antonov, J. I., Boyer, T. P., Garcia, H. E., Baranova, O. K., Zweng, M. M., and Johnson, D. R.: World ocean atlas 2009, volume 1: temperature, in: NOAA Atlas Nesdis 68, edited by: Levitus, S., US Government Printing Office, Washington, DC, 184, 2010.

Mahowald, N. M., Baker, A. R., Bergametti, G., Brooks, N., Duce, R. A., Jickells, T. D., Kubilay, N., Prospero, J. M., and Tegen, I.: Atmospheric global dust cycle and iron inputs to the ocean, Global Biogeochem. Cy., 19, GB4025, doi:10.1029/2004gb002402, 2005a.

Mahowald, N. M., Baker, A. R., Bergametti, G., Brooks, N., Duce, R. A., Jickells, T. D., Kubilay, N., Prospero, J. M., and Tegen, I.: Atmospheric global dust cycle and iron inputs to the ocean, Global Biogeochem. Cy., 19, GB4025, doi:10.1029/2004GB002402, 2005b.

Mahowald, N. M., Muhs, D. R., Levis, S., Rasch, P. J., Yoshioka, M., Zender, C. S., and Luo, C.: Change in atmospheric mineral aerosols in response to climate: last glacial period, preindustrial, modern, and doubled carbon dioxide climates, J. Geophys. Res., 111, D10202, doi:10.1029/2005jd006653, 2006.

Mahowald, N. M., Engelstaedter, S., Luo, C., Sealy, A., Artaxo, P., Benitez-Nelson, C., Bonnet, S., Chen, Y., Chuang, P. Y., Cohen, D. D., Dulac, F., Herut, B., Johansen, A. M., Kubilay, N., Losno, R., Maenhaut, W., Paytan, A., Prospero, J. A., Shank, L. M., and Siefert, R. L.: Atmospheric iron deposition: global distribution, variability, and human perturbations, in: Annual Review of Marine Science, Annual Reviews, Palo Alto, 245–278, 2009.

Mariotti, A., Germon, J., Hubert, P., Kaiser, P., Letolle, R., Tardieux, A., and Tardieux, P.: Experimental determination of nitrogen kinetic isotope fractionation: some principles; illustration for the denitrification and nitrification processes, Plant Soil, 62, 413–430, doi:10.1007/bf02374138, 1981.

McElroy, M. B.: Marine biological controls on atmospheric CO_2 and climate, Nature, 302, 328–329, 1983.

Middelburg, J. J., Soetaert, K., Herman, P. M. J., and Heip, C. H. R.: Denitrification in marine sediments: a model study, Global Biogeochem. Cy., 10, 661–673, doi:10.1029/96gb02562, 1996.

Mohr, W., Großkopf, T., Wallace, D. W. R., and LaRoche, J.: Methodological underestimation of oceanic nitrogen fixation rates, PLoS ONE, 5, e12583, 2010.

Monteiro, F. M., Dutkiewicz, S., and Follows, M. J.: Biogeographical controls on the marine nitrogen fixers, Global Biogeochem. Cy., 25, GB2003, doi:10.1029/2010gb003902, 2011.

Montoya, J. P., Holl, C. M., Zehr, J. P., Hansen, A., Villareal, T. A., and Capone, D. G.: High rates of N_2 fixation by unicellular diazotrophs in the oligotrophic pacific ocean, Nature, 430, 1027–1032, 2004.

Moore, J. K. and Doney, S. C.: Iron availability limits the ocean nitrogen inventory stabilizing feedbacks between marine denitrification and nitrogen fixation, Global Biogeochem. Cy., 21, GB2001, doi:10.1029/2006gb002762, 2007.

Moore, J. K., Doney, S. C., and Lindsay, K.: Upper ocean ecosystem dynamics and iron cycling in a global three-dimensional model, Global Biogeochem. Cy., 18, GB4028, doi:10.1029/2004gb002220, 2004.

Mulholland, M. R.: The fate of nitrogen fixed by diazotrophs in the ocean, Biogeosciences, 4, 37–51, doi:10.5194/bg-4-37-2007, 2007.

Mulholland, M. R., Ohki, K., and Capone, D. G.: Nutrient controls on nitrogen uptake and metabolism by natural populations and cultures of *trichodesmium* (cyanobacteria), J. Phycol., 37, 1001–1009, 2001.

Pandey, K. D., Shukla, S. P., Shukla, P. N., Giri, D. D., Singh, J. S., Singh, P., and Kashyap, A. K.: Cyanobacteria in antarctica: ecology, physiology and cold adaptation, Cell. Mol. Biol., 50, 575–584, 2004.

Robinson, R. S., Kienast, M., Luiza Albuquerque, A., Altabet, M., Contreras, S., De Pol Holz, R., Dubois, N., Francois, R., Galbraith, E., Hsu, T.-C., Ivanochko, T., Jaccard, S., Kao, S.-J., Kiefer, T., Kienast, S., Lehmann, M., Martinez, P., McCarthy, M., Möbius, J., Pedersen, T., Quan, T. M., Ryabenko, E., Schmittner, A., Schneider, R., Schneider-Mor, A., Shigemitsu, M., Sinclair, D., Somes, C., Studer, A., Thunell, R., and Yang, J.-Y.: A review of nitrogen isotopic alteration in marine sediments, Paleoceanography, 27, PA4203, doi:10.1029/2012pa002321, 2012.

Ryabenko, E., Kock, A., Bange, H. W., Altabet, M. A., and Wallace, D. W. R.: Contrasting biogeochemistry of nitrogen in the Atlantic and Pacific Oxygen Minimum Zones, Biogeosciences, 9, 203–215, doi:10.5194/bg-9-203-2012, 2012.

Sanudo-Wilhelmy, S. A., Tovar-Sanchez, A., Fu, F.-X., Capone, D. G., Carpenter, E. J., and Hutchins, D. A.: The impact of surface-adsorbed phosphorus on phytoplankton redfield stoichiometry, Nature, 432, 897–901, http://www.nature.com/nature/journal/v432/n7019/abs/nature03125.html#supplementary-information, 2004.

Schmittner, A., Oschlies, A., Giraud, X., Eby, M., and Simmons, H. L.: A global model of the marine ecosystem for long-term simulations: sensitivity to ocean mixing buoyancy forcing, particle sinking, and dissolved organic matter cycling, Global Biogeochem. Cy., 19, doi:10.1029/2004GB002283, 2005.

Schmittner, A., Oschlies, A., Matthews, H. D., and Galbraith, E. D.: Future changes in climate, ocean circulation, ecosystems, and biogeochemical cycling simulated for a business-as-usual CO_2 emission scenario until year 4000 ad, Global Biogeochem. Cy., 22, GB1013, doi:10.1029/2007gb002953, 2008a.

Schmittner, A., Oschlies, A., Matthews, H. D., and Galbraith, E. G.: Future changes in climate, ocean circulation, ecosystems, and biogeochemical cycling simulated for a buisness-as-usual CO_2 emission scenario until year 4000 ad, Global Biogeochem. Cy., 22, GB1013, doi:10.1029/2007GB002953, 2008b.

Sigman, D. M., Altabet, M. A., McCorkle, D. C., Francois, R., and Fischer, G.: The d^{15}N of nitrate in the southern ocean: nitrogen cycling and circulation in the ocean interior, J. Geophys. Res., 105, 19599–19614, doi:10.1029/2000jc000265, 2000.

Simmons, H. L., Jayne, S. R., Laurent, L. C. S., and Weaver, A. J.: Tidally driven mixing in a numerical model of the ocean general circulation, Ocean Model., 6, 245–263, doi:10.1016/S1463-5003(03)00011-8, 2004.

Somes, C. J., Schmittner, A., and Altabet, M. A.: Nitrogen isotope simulations show the importance of atmospheric iron deposition for nitrogen fixation across the pacific ocean, Geophys. Res. Lett., 37, L23605, doi:10.1029/2010gl044537, 2010a.

Somes, C. J., Schmittner, A., Galbraith, E. D., Lehmann, M. F., Altabet, M. A., Montoya, J. P., Letelier, R. M., Mix, A. C., Bourbonnais, A., and Eby, M.: Simulating the global distribution of nitrogen isotopes in the ocean, Global Biogeochem. Cy., 24, GB4019, doi:10.1029/2009gb003767, 2010b.

Sterner, R. W. and Elser, J. J.: Ecological stoichiometry: the biology of elements from molecules to the biosphere, Princeton University Press, 429 pp., 2002.

Tesdal, J.-E., Galbraith, E. D., and Kienast, M.: Nitrogen isotopes in bulk marine sediment: linking seafloor observations with subseafloor records, Biogeosciences, 10, 101–118, doi:10.5194/bg-10-101-2013, 2013.

Thamdrup, B. and Dalsgaard, T.: Production of N_2 through anaerobic ammonium oxidation coupled to nitrate reduction in marine sediments, Appl. Environ. Microbiol., 68, 1312–1318, 2002.

Voss, M., Dippner, J. W., and Montoya, J. P.: Nitrogen isotope patterns in the oxygen-deficient waters of the eastern tropical north pacific ocean, Deep-Sea Res. Pt. I, 48, 1905–1921, 2001.

Ward, B. B., Devol, A. H., Rich, J. J., Chang, B. X., Bulow, S. E., Naik, H., Pratihary, A., and Jayakumar, A.: Denitrification as the dominant nitrogen loss process in the arabian sea, Nature, 461, 78–81, doi:10.1038/nature08276, 2009.

Weaver, A. J., Eby, M., Wiebe, E. C., Bitz, C. M., Duffy, P. B., Ewen, T. L., Fanning, A. F., Holland, M. M., MacFadyen, A., Matthews, H. D., Meissner, K. J., Saenko, O., Schmittner, A., Wang, H., and Yoshimori, M.: The uvic earth system climate model: Model description, climatology, and applications to past, present and future climates, Atmos.-Ocean, 39, 361–428, 2001.

Zehr, J. P.: Nitrogen fixation by marine cyanobacteria, Trends Microbiol., 19, 162–173, 2011.

Table 1. Model experiment parameter settings.

Experiment	lim WCD (μM NO_3^-)	ε_{BD} (‰)	α_{BD}	ω_{Diaz} $(\text{mmol m}^{-3})^{-2}\,\text{d}^{-1}$	ν_{Diaz} d^{-1}
1	20	0	1.35	0.11	0.25
2	26	0	1.55	0.1	0.25
3	32	0	1.5	0.15	0.25
4	32	2	1.9	0.078	0.25
5	32	4	3.2	0.001	0.17

See text and Table A1 for additional details.

Table 2. Model sensitivity experiment results.

Experiment			Global Results							Suboxic Zone Results		
#	lim WCD (μM NO_3^-)	ε_{BD} (‰)	N_2 fixation (Tg N yr^{-1})	WC Deni. (Tg N yr^{-1})	Benthic Deni. (Tg N yr^{-1})	Benthic : WC Deni.	NO_3^- (30.8 μM)	Deep ocean $\delta^{15}NO_3^-$ (5.0 ‰)	Global ocean $\delta^{15}NO_3^-$ (~ 5.5 ‰)	NO_3^- (33.5 μM)	$\delta^{15}NO_3^-$ (~ 12 ‰)	$NO_3 : 15PO_4$ (0.760)
1	20	0	248	140	108	0.77	31.0	4.95	5.51	24.8	17.5	0.549
2	26	0	232	109	123	1.13	30.8	5.01	5.59	28.7	15.9	0.635
3	32	0	203	86.4	117	1.39	30.2	5.01	5.59	33.3	14.1	0.722
4	32	2	225	75.7	149	1.96	30.6	5.01	5.53	33.2	13.6	0.734
5	32	4	342	75.6	267	3.53	30.4	5.06	5.45	32.9	11.9	0.789

Model results for the different sensitivity experiments in the global ocean and suboxic zone ($O_2 < 10\,\mu$M) with the observational estimate given in parenthesis.

Table 3. Measures of seafloor δ^{15}N model performance[a] with the observational average given in parenthesis.

Experiment			Seafloor δ^{15}N Evaluation											
			Southern Ocean						Global Ocean					
#	lim WCD (μM NO_3^-)	ε_{BD} (‰)	Sinking PON full mean (%)	Seafloor full mean	Seafloor Data-masked mean (5.33 ‰)	*R*	STD	RMS	Sinking PON full mean (%)	Seafloor full mean	Seafloor data-masked mean (7.00 ‰)	*R*	STD	RMS
1	20	0	1.93	5.37	5.27	0.387	1.24	1.26	4.26	7.63	7.67	0.503	1.93	1.70
2	26	0	2.04	5.45	5.38	0.391	1.25	1.26	4.37	7.73	7.46	0.553	1.6	1.35
3	32	0	2.20	5.61	5.54	0.391	1.26	1.29	4.22	7.58	6.95	0.584	1.18	1.01
4	32	2	2.08	5.48	5.41	0.410	1.25	1.24	4.12	7.48	6.76	0.593	1.08	0.957
5	32	4	2.01	5.42	5.35	0.410	1.23	1.23	3.63	6.99	6.28	0.592	0.975	0.968

[a] Statistical measures are correlation coefficient (*R*), standard deviation (STD), and root mean squared (RMS) error normalized by the standard deviation of the observations in the global seafloor. Note "full mean" refers to the entire ocean basin, whereas "data-masked mean" only include grid points where observations exist.

Title Page
Abstract | Introduction
Conclusions | References
Tables | Figures
◀| |▶
◀ ▶
Back | Close
Full Screen / Esc
Printer-friendly Version
Interactive Discussion

Table 4. δ^{15}N box model parameter list.

	$\varepsilon_{\mathrm{Nfix}}$ (‰)	WCD rate (Tg N yr^{-1})	$\varepsilon_{\mathrm{WCD}}$ (‰)	WCD zone $\delta^{15}\mathrm{NO}_3^-$ (‰)	$\varepsilon_{\mathrm{BD}}$ (‰)	BD zone $\delta^{15}\mathrm{NO}_3^-$ (‰)	BD : WCD (one-box model)	BD : WCD (reported)
B&D02[a]	1	75	25	5	1.5	5	4.31	3.73
DEU04	0	70	25	12	0	5	2.69	2.71
ALT07[b]	1	90	25	18	0	5	1.01	~ 1.00
lim WCD = 20, $\varepsilon_{\mathrm{BD}} = 0$	1.5	144	25	18.2	0	5.86	0.787	0.757
lim WCD = 26, $\varepsilon_{\mathrm{BD}} = 0$	1.5	112	25	15.7	0	5.79	1.13	1.13
lim WCD = 32, $\varepsilon_{\mathrm{BD}} = 0$	1.5	87.6	25	13.8	0	5.74	1.40	1.39
lim WCD = 32, $\varepsilon_{\mathrm{BD}} = 2$	1.5	78.3	25	13.4	2	5.88	1.96	1.96
lim WCD = 32, $\varepsilon_{\mathrm{BD}} = 4$	1.5	77.0	25	11.6	4	5.96	3.58	3.53

[a] Brandes and Devol (2002) reported ratio also included isotope effects from atmospheric N deposition, river input, and sediment burial, which are excluded in the one-box model calculation to maintain consistency with the other model configurations. These processes slightly reduce the BD : WCD ratio and suggests the other model estimates may be slightly overestimating BD : WCD as well.

[b] Altabet (2007) used a combination of reducing the fractionation factor of water column denitrification (to account for circulation effects not included in the one-box model) and increasing water column denitrification zone $\delta^{15}\mathrm{NO}_3^-$ so the δ^{15}N value of nitrogen removed was −7 ‰. We leave $\varepsilon_{\mathrm{WD}}$ at 25 ‰ and increase the water column denitrification zone $\delta^{15}\mathrm{NO}_3^-$ to 18 ‰ achieve his suggested δ^{15}N value of −7 ‰ for nitrogen removal.

Table A1. Marine ecosystem – biogeochemical parameter list.

Parameter	Symbol	Value	Units
Phytoplankton (P_O, P_D) Coefficients			
Initial slope of *P*-*I* curve	α	0.1	$(\mathrm{W\,m^{-2}})^{-1}\,\mathrm{d^{-1}}$
Photosynthetically active radiation	PAR	0.43	
Light attenuation in water	k_w	0.04	$\mathrm{m^{-1}}$
Light attenuation through phytoplankton	k_c	0.03	$\mathrm{m^{-1}(mmol\,m^{-3})^{-1}}$
Light attenuation through sea ice	k_i	5	$\mathrm{m^{-1}}$
Half-saturation constant for N uptake	k_N	0.7	$\mathrm{mmol\,m^{-3}}$
Phytoplankton specific mortality rate	ν_{PO}	0.025	$\mathrm{d^{-1}}$
Maximum growth rate (at 0 °C)*	a_O	0.35	$\mathrm{d^{-1}}$
Phytoplankton fast-recycling rate	μ_{P0}	0.014	$\mathrm{d^{-1}}$
Diazotrophs' handicap	c_{Diaz}	0.13	$\mathrm{d^{-1}}$
Diaztoroph specific mortality rate	ν_{Diaz}	0.025	$\mathrm{d^{-1}}$
Diazotroph fast-recycling rate	μ_{D0}	0.0016	$\mathrm{d^{-1}}$
Zooplankton (Z) Coefficients			
Assimilation efficiency	γ	0.925	
Maximum grazing rate	g	1.575	$\mathrm{d^{-1}}$
Phytoplankton prey-capture rate	ϖ_O	5.0	$\mathrm{(mmol\,m^{-3})^{-2}\,d^{-1}}$
Diazotroph prey-capture rate	ϖ_{Diaz}	0.125	$\mathrm{(mmol\,m^{-3})^{-2}\,d^{-1}}$
Mortality	μ_{Z_0}	0.34	$\mathrm{(mmol\,m^{-3})^{-2}\,d^{-1}}$
Excretion	ν_Z	0.015	$\mathrm{d^{-1}}$
Detritus (D) Coefficients			
Remineralization rate	μ_{D0}	0.065	$\mathrm{d^{-1}}$
Sinking speed at surface	w_{D0}	13	$\mathrm{m\,d^{-1}}$
Increase of sinking speed with depth	m_w	0.06	$\mathrm{d^{-1}}$
E-folding temperature of biological rates	T_b	15.65	°C
Elemental Ratios			
Molar Oxygen : Nitrogen	$R_{\mathrm{O:N}}$	10.6	
Molar Carbon : Nitrogen	$R_{\mathrm{C:N}}$	6.625	
Phytoplankton Nitrogen : Phosphorus	$\mathrm{Phyt_{N:P}}$	16	
Diazotroph Nitrogen : Phosphorus	$\mathrm{Diaz_{N:P}}$	40	
Zooplankton Nitrogen : Phosphorus	$\mathrm{Zoop_{N:P}}$	16	

* Marine ecosystem-biogeochemistry parameter list for experiment 3 (lim WCD = 32, $\varepsilon_{\mathrm{BD}} = 0$). See Table 2 for changes to parameters for other experiments.

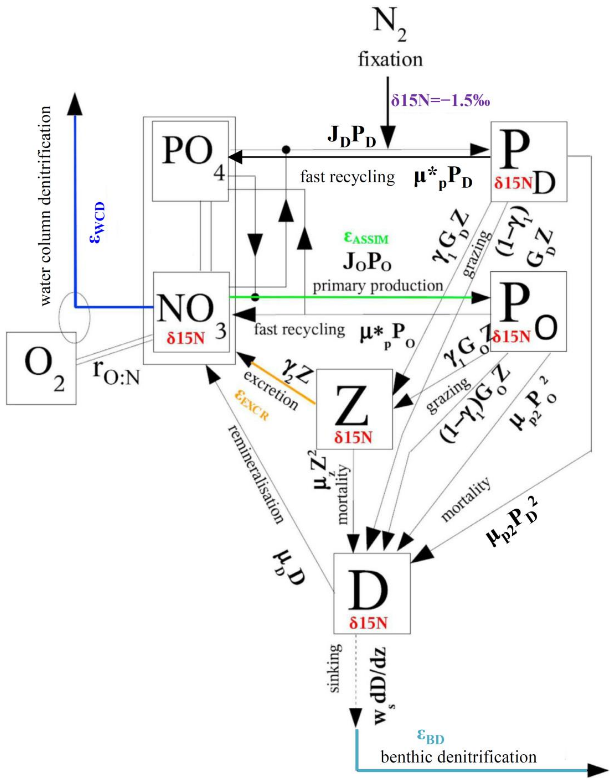

Fig. 1. Schematic of the marine ecosystem/biogeochemical model compartments including the nitrogen isotope parameters (colors).

Title Page
Abstract
Introduction
Conclusions
References
Tables
Figures
◀▮
▶▮
◀
▶
Back
Close
Full Screen / Esc
Printer-friendly Version
Interactive Discussion

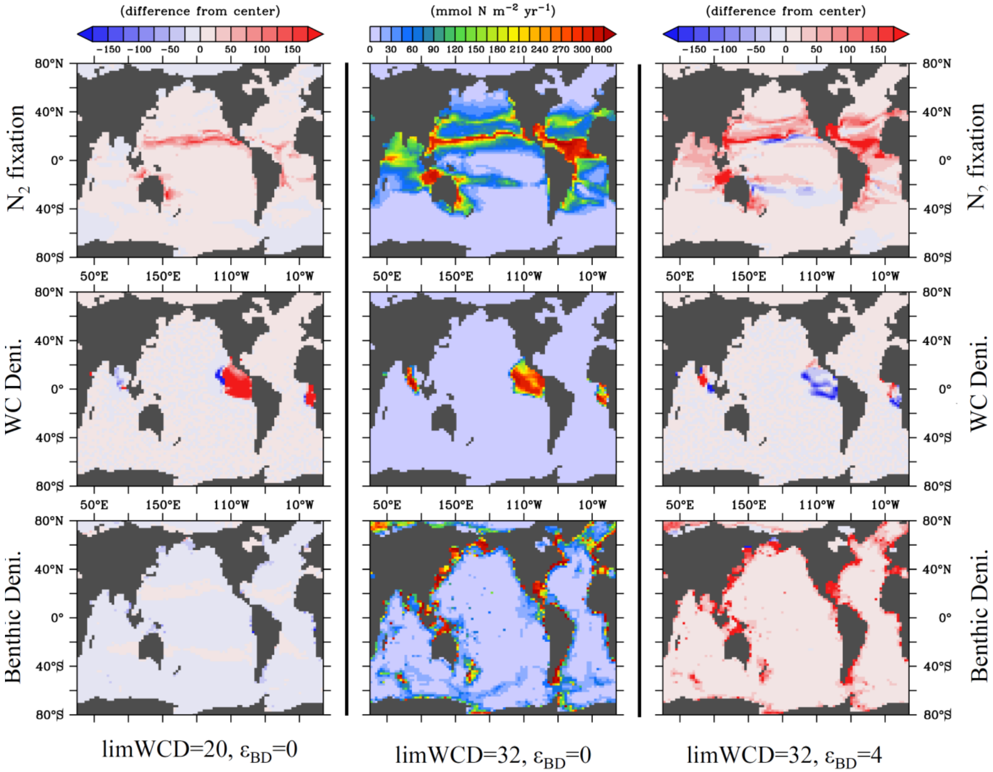

Fig. 2. Global distribution of annual vertically integrated N_2 fixation (top row), water column denitrification (middle row) and benthic denitrification (bottom row) for the experiments lim WCD = 20, $\varepsilon_{BD} = 0$ (left), lim WCD = 32, $\varepsilon_{BD} = 0$ (center), and lim WCD = 32, $\varepsilon_{BD} = 4$ (right). See text for model experiment details.

Title Page
Abstract | Introduction
Conclusions | References
Tables | Figures
◀| |▶
◀ ▶
Back | Close
Full Screen / Esc
Printer-friendly Version
Interactive Discussion

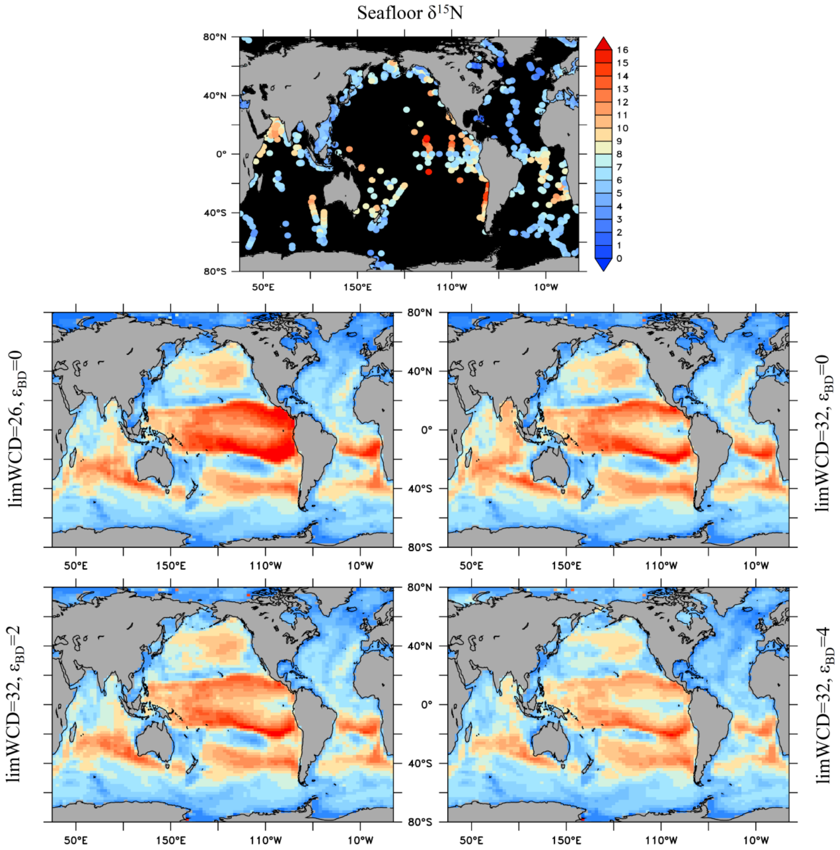

Fig. 3. Seafloor δ^{15}N (Tesdal et al., 2013) comparison with model experiments lim WCD = 26, ε_{BD} = 0 and lim WCD = 32, ε_{BD} = 0, 2, 4. Note a simple diagenetic model was applied to model sinking δ^{15}N to account for diagenetic alteration during burial into the seafloor sediments based on seafloor depth (Robinson et al., 2012). See text for additional details.

Title Page
Abstract | Introduction
Conclusions | References
Tables | Figures
|◀ | ▶|
◀ | ▶
Back | Close
Full Screen / Esc
Printer-friendly Version
Interactive Discussion

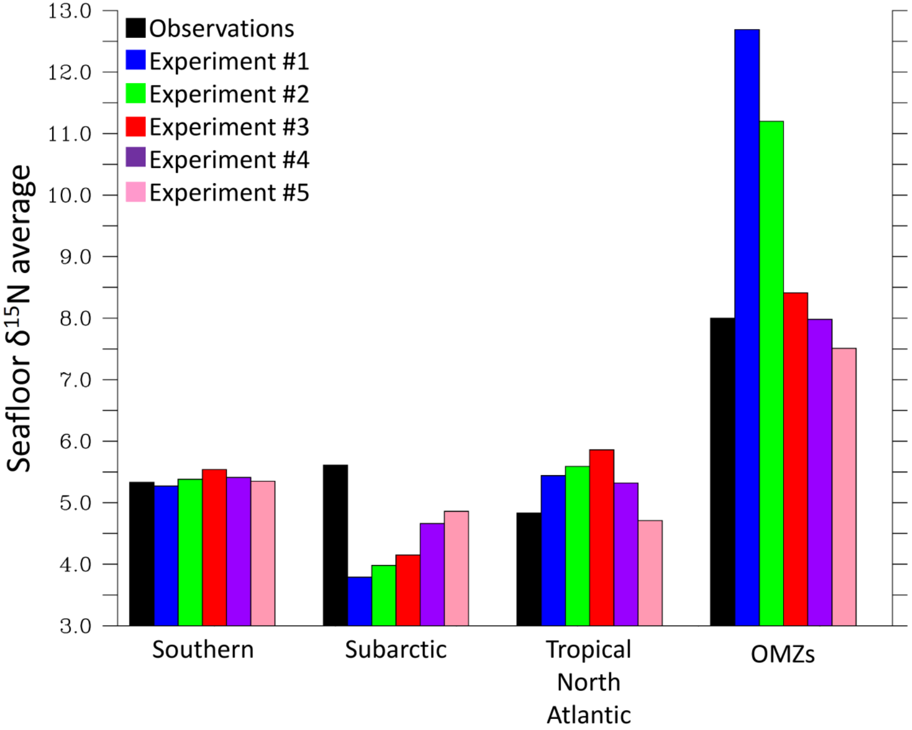

Fig. 4. Comparison of average seafloor δ^{15}N in the Southern Ocean (50° S–75° S), Subarctic/Arctic Ocean (50° N–75° N), Tropical North Atlantic (0° N–25° N), and oxygen minimum zones ($O_2 < 10\,\mu M$). Note we also include locations of observed OMZs to account for the displaced model OMZs in this comparison.

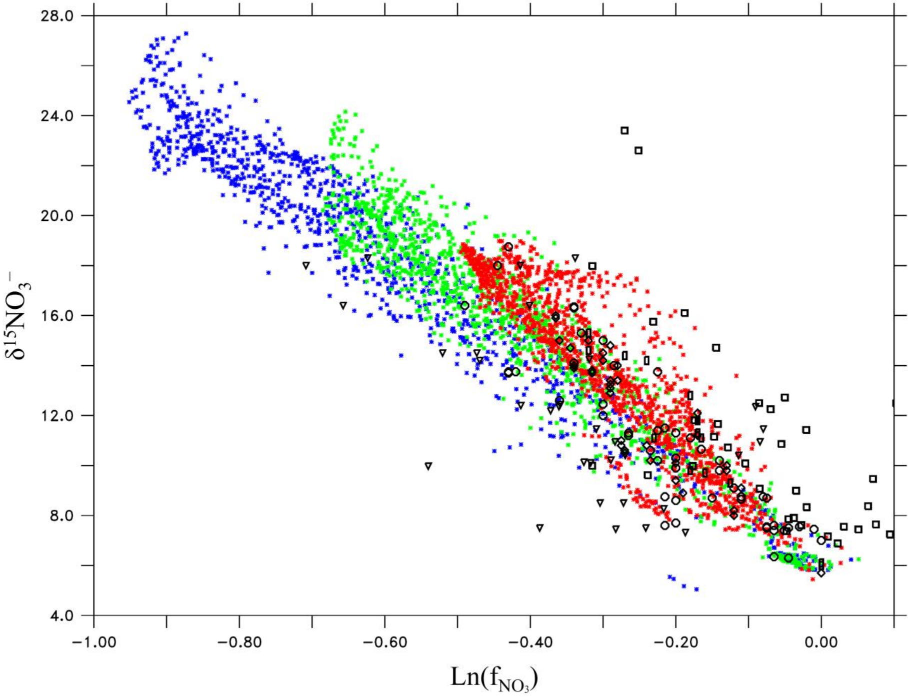

Fig. 5. Annual mean $\delta^{15}NO_3^-$ versus expected nitrate (f_{NO_3}) shows the increase of $\delta^{15}NO_3^-$ as NO_3^- is consumed in suboxic zones ($O_2 < 10\,\mu M$) from the isotope effect of water column N-loss in lim WCD = 20 (blue), lim WCD = 26 (green), lim WCD = 32 (red) and observations (black) from Cline and Kaplan (1975) ([]), Altabet et al. (1995) (Δ), Brandes et al. (1998) (◊), Voss et al. (2001) (◯), and Somes et al. (2010b) (□). Note $\varepsilon_{BD} = 0$ ‰ for the model experiments shown here. Expected nitrate is determined to be at the elemental ratio $15 \cdot PO_4^{3-}$ in the model based on experiments where water column denitrification was switched off (not shown), which is in agreement with the expected nitrate calculation from Voss et al. (2001) based on nitrate-density isopycnals. Observations near the seafloor are excluded to avoid any impact from benthic denitrification.

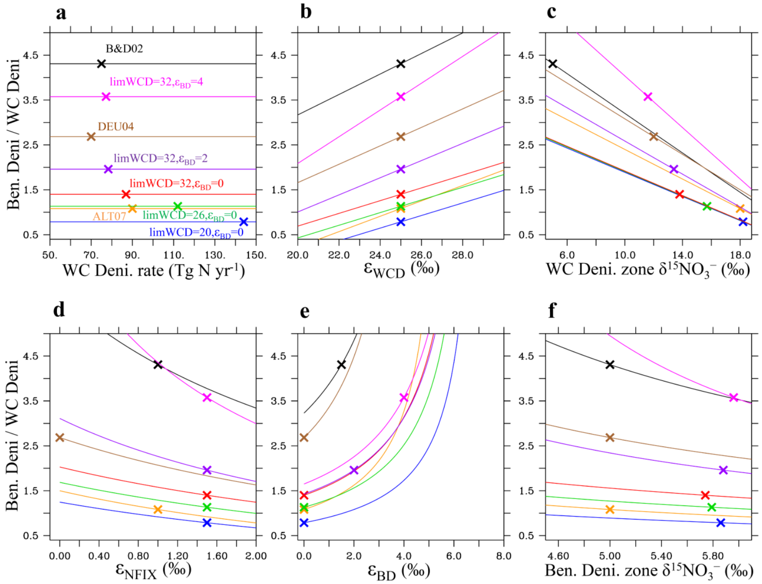

Fig. 6. Results of the one-box $\delta^{15}NO_3^-$ model with different nitrogen isotope parameter settings according to previous configurations (Brandes and Devol, 2002; Deutsch et al., 2004; Altabet, 2007) and this study (Table 4). Each panel shows the sensitivity of one parameter on the ratio of benthic denitrification to water column denitrification (BD : WCD) needed to achieve observed mean $\delta^{15}NO_3^-$ in a steady-state scenario while all other parameters are held constant: **(a)** water column denitrification rate, **(b)** water column denitrification fractionation factor (ε_{WCD}), **(c)** average $\delta^{15}NO_3^-$ value where water column denitrification occurs, and **(d)** N_2 fixation fractionation factor (ε_{Nfix}), **(e)** benthic denitrification fractionation factor (ε_{BD}), and **(f)** average $\delta^{15}NO_3^-$ value where benthic denitrification occurs. Note ε_{Nfix} makes diazotroph biomass depleted in $\delta^{15}N$ by this value. The crosses (X) show the parameter chosen for each reported model configuration and denotes the benthic to water column denitrification ratio of the previous studies as well as coupled three-dimensional experiments from this study.

Title Page
Abstract
Introduction
Conclusions
References
Tables
Figures
◀I
▶I
◀
▶
Back
Close
Full Screen / Esc
Printer-friendly Version
Interactive Discussion

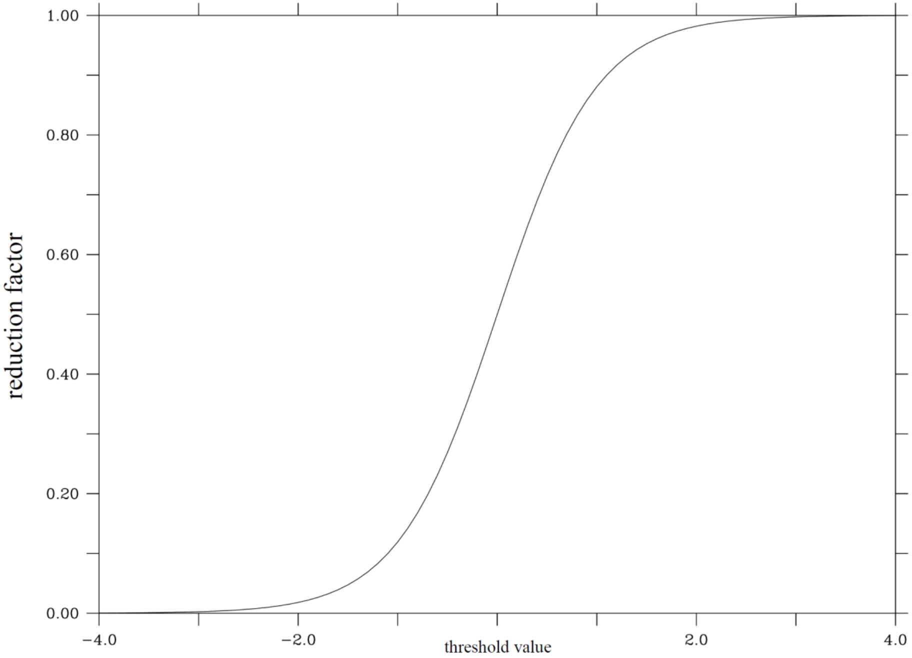

Fig. B1. Reduction factor applied to water column denitrification for given NO_3^- concentration (µM) thresholds.

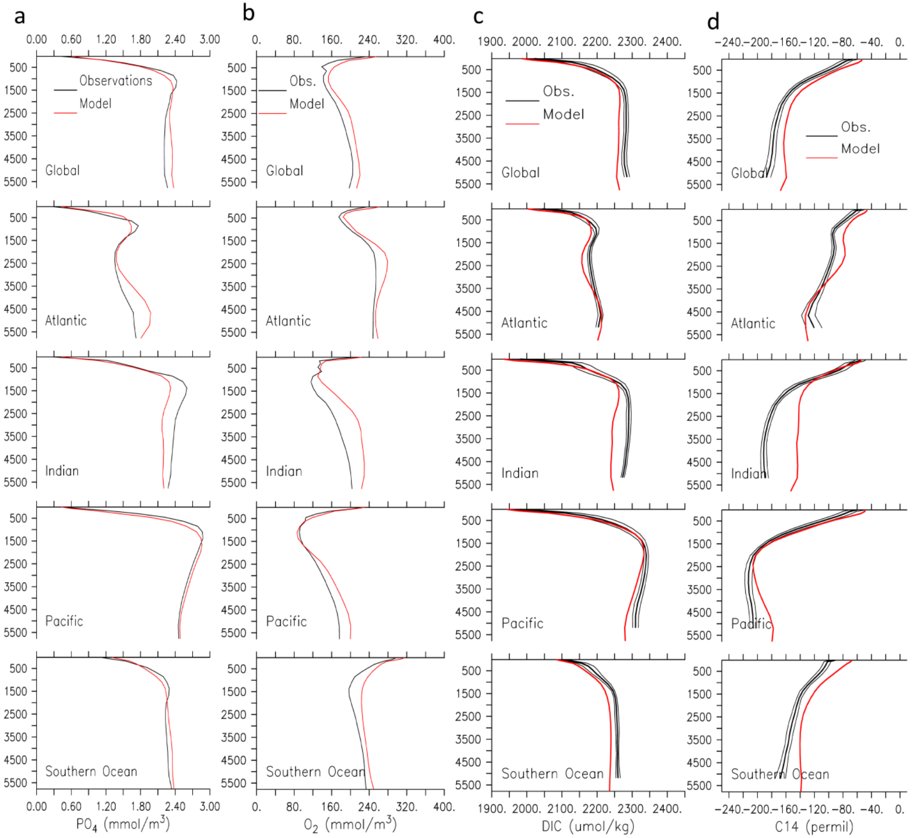

Fig. B2. Basin-scale model-data comparison of **(a)** PO_4^-, **(b)** O_2, **(c)** apparent oxygen utilization (AOU), and **(d)** $\Delta^{14}C$ with lim WCD = 32, $\varepsilon_{BD} = 2$ model experiment.